Characterization of the electron acceptors of the

Type-I photosynthetic reaction center of *Heliobacterium modesticaldum*

by

John Cowgill

A Thesis Presented in Partial Fulfillment
of the Requirements for the Degree
Master of Science

Approved October 2012 by the
Graduate Supervisory Committee:

Kevin Redding, Chair
Anne Jones
Petra Fromme

ARIZONA STATE UNIVERSITY

December 2012

ABSTRACT

The heliobacterial reaction center (HbRC) is widely considered the simplest and most primitive photosynthetic reaction center (RC) still in existence. Despite the simplicity of the HbRC, many aspects of the electron transfer mechanism remain unknown or under debate. Improving our understanding of the structure and function of the HbRC is important in determining its role in the evolution of photosynthetic RCs. In this work, the function and properties of the iron-sulfur cluster F_X and quinones of the HbRC were investigated, as these are the characteristic terminal electron acceptors used by Type-I and Type-II RCs, respectively. In Chapter 3, I develop a system to directly detect quinone double reduction activity using reverse-phase high pressure liquid chromatography (RP-HPLC), showing that Photosystem I (PSI) can reduce PQ to PQH_2. In Chapter 4, I use RP-HPLC to characterize the HbRC, showing a surprisingly small antenna size and confirming the presence of menaquinone (MQ) in the isolated HbRC. The terminal electron acceptor F_X was characterized spectroscopically and electrochemically in Chapter 5. I used three new systems to reduce F_X in the HbRC, using EPR to confirm a S=3/2 ground-state for the reduced cluster. The midpoint potential of F_X determined through thin film voltammetry was -372 mV, showing the cluster is much less reducing than previously expected. In Chapter 7, I show light-driven reduction of menaquinone in heliobacterial membrane samples using only mild chemical reductants. Finally, I discuss the evolutionary implications of these findings in Chapter 7.

ACKNOWLEDGMENTS

TABLE OF CONTENTS

LIST OF TABLES

LIST OF FIGURES

LIST OF ABBREVIATIONS

Abbreviation	Definition
4Fe-4S	Four iron and four sulfur cluster
A_0	Primary acceptor of PSI or the HbRC
A_1	Secondary acceptor of PSI
Bchl	Bacteriochlorophyll
Chl	Chlorophyll
CW-EPR	Continuous wave electron paramagnetic resonance
D, E	Axial and rhombic zero-field splitting parameters
DDM	Dodecyl maltoside
DMPC	Diimyristoyl phosphorylcholine
ESEEM	Electron spin echo envelope modulation
F_A/F_B, F_X	Iron-sulfur clusters in Type-I reaction centers
GbRC	Green-sulfur bacterial reaction center
HbRC	Heliobacterial reaction center
IRF	Instrument response factor
MES	2-(N-morpholino) ethanosulfonic acid
MOPS	3-(N-morpholino) propansulfonic acid
MQ	Menaquinone
MQH_2	Menaquinol
P700, P800	Primary donors of PSI and the HbRC
PhQ	Phylloquinone
PQ	Plastoquinone
PQH_2	Plastoquinol
PsaA, PsaB	Peptide components of core heterodimer of PSI
PsaC	Bacterial ferredoxin subunit of PSI
PshA	Peptide component of core homodimer of HbRC

Abbreviation	Definition
PshB	Bacterial ferredoxin that associates with HbRC *in vivo*
Q_A, Q_B	Quinone binding sites of Type-II reaction centers
RC	Reaction center
RP-HPLC	Reverse-phase high pressure liquid chromatography
SDT	Sodium dithionite
TC-SPC	Time-correlated single-photon counting
Tris	Tris(hydroxymethyl) aminomethane

CHAPTER 1: INTRODUCTION

Photosynthesis

Photosynthesis is the process in which light energy is harvested and used to drive important chemical reactions by living organisms. The nature of these chemical reactions vary even within a given organism depending on the metabolic needs of the cell, but the most well known are found in oxygenic photosynthesis. These can further be divided into the "light" and "dark" reactions. In the light reactions, energy from absorbed photons is used to drive the formation of high-energy compounds such as ATP and NADPH. These compounds are consumed in the dark reactions, forming sugars and other stable storage molecules for chemical energy (*1*).

As implied above, there are other forms of photosynthesis that do involve oxygen production that are collectively referred to as anoxygenic photosynthesis. While the overall processes vary significantly between organisms, the initial steps where light energy is converted into chemical energy are very similar.

Photosynthetic reaction centers

The light reactions described above rely on pigment-binding protein complexes referred to as photosynthetic reaction centers (RCs). Antenna pigment molecules like chlorophylls and carotenoids absorb light energy in the form of photons. This generates high-energy excited states, which ultimately give rise to a charge separated state. There are strong similarities in the initial charge separated states between all RCs. A "special pair" of chlorophylls becomes oxidized, forming a cation radical that is delocalized between the pair. The electron ejected from the special pair reduces a primary acceptor. The primary acceptor is either chlorophyll or pheophytin (a chlorophyll with no Mg^{2+}). Eventually the electron is used to reduce a terminal electron acceptor, which differs depending on the type of RC. There are currently two classes of photosynthetic RCs described that are defined by their terminal electron acceptor (*2*).

Type-I

Type-I RCs utilize iron-sulfur clusters as terminal electron acceptors. There are four known Type-I RCs; Photosystem I of oxygenic photosynthetic organisms (plants, algae, and cyanobacteria), the Green-sulfur bacterial reaction center (GbRC), the heliobacterial reaction center (HbRC), and the reaction center of the newly discovered Chloroacidobacteria. Of the Type-I RCs, Photosystem I (PSI) is the most extensively characterized and the only one for which an X-ray crystal structure is available (*3*).

The simplified mechanism of Photosystem I is illustrated in Figure 1 below. Light energy that is absorbed by antenna chlorophylls (not shown) is funneled to the special pair of chlorophyll *a* referred to as P700 through resonance energy transfer. This energy drives the oxidation of P700 and the reduction of the primary acceptor A_0, another chlorophyll *a*. The primary acceptor then reduces a secondary acceptor (A_1), which is a tightly bound phylloquinone (PhQ) (*4*). The semiquinone radical generated in this step is very unstable, and quickly reduces the 4Fe-4S cluster F_X (*5*). The electron leaves PSI through a chain of 4Fe-4S clusters and reduces soluble electron acceptors such as ferredoxin or flavodoxin.

The Type-I RCs from anoxygenic bacteria will be discussed further in the section titled Heliobacterial reaction center.

Type-II

Type-II RCs use quinones as terminal electron acceptors, doubly reducing them to the stable hydroquinone (or quinol) form. The three known Type-II RCs are Photosystem II (found in plants, algae, and cyanobacteria), the Purple-bacterial reaction center (PbRC), and the reaction center of Green-sliding bacteria. While crystal structures are available for both Photosystem II and the PbRC, the PbRC has historically been the most extensively studied Type-II RC (*6*).

The mechanism of the PbRC is shown in Figure 1 below. Similar to PSI, a special pair of bacteriochlorophyll serves as the primary donor in the PbRC and other

2
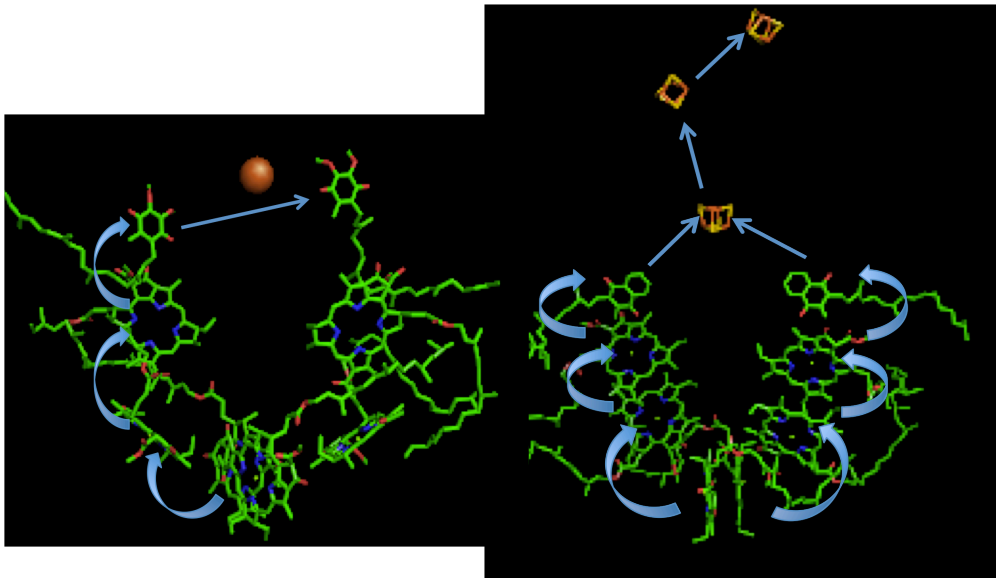
Figure 1. Electron transfer mechanisms of model Type-I (right) and II (left) photosynthetic reaction centers. Arrows denote movement of electrons for the PbRC (left) and PSI (right). Note that Photosystem I (1JB0) has two functionally symmetric branches while the PbRC (1AIJ) is functionally asymmetric.

Type-II RCs. Unlike PSI, the primary acceptor in Type-II RCs is a pheophytin (or bacteriopheophytin). A tightly bound quinone serves as a secondary acceptor at the Q_A site while a loosely bound quinone serves as the terminal electron acceptor at the Q_B site (*7, 8*). Type-II RCs require two photons, causing transfer of two electrons to the quinone at the Q_B site. The doubly reduced quinone takes up two protons and can diffuse from the binding site. An important note is that while PSI uses two functionally symmetric branches, Type-II RCs have functionally distinct branches (*9*). The B-branch stabilizes the semiquinone state of Q_B while the A-branch is involved in electron transfer reactions (*10*).

Evolution

Structural similarities between PSI, PSII, and the PbRC were immediately recognized after the crystal structures of each were published (*3, 11, 12*). Figure 2

Photosystem II (3ARC) PbRC (1AIJ) Photosystem I (1JB0)

Side view

Top view
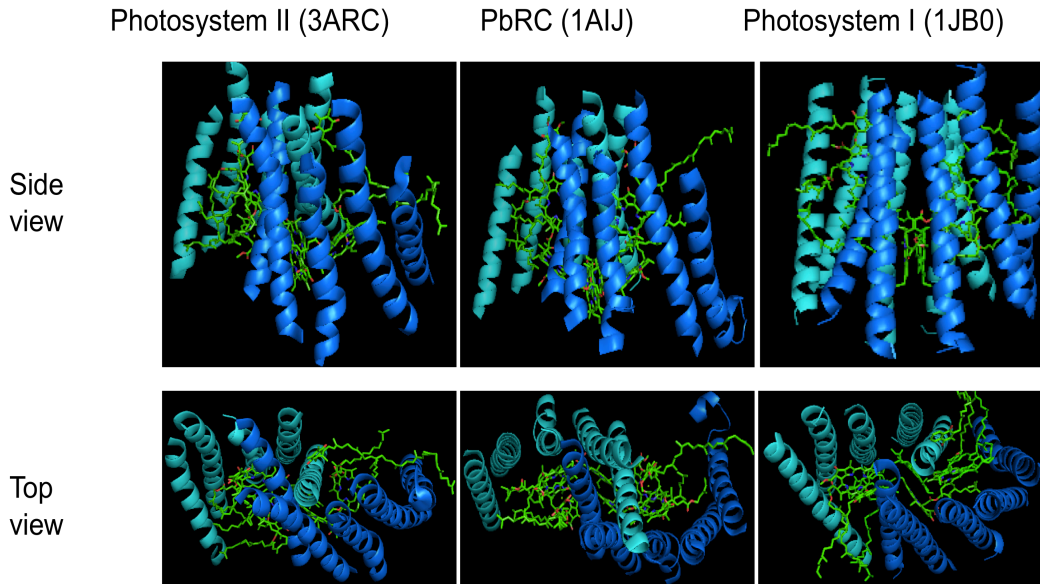
Figure 2. Structures of the 10 transmembrane helices and organic cofactors that make up the core reaction center for PSII (left), the PbRC (middle), and PSI (right).

shows the strong structural homology in 10 transmembrane helices, coming from two polypeptides that constitute the core of these three RCs. These helices form a pseudo-symmetric "cage" around the electron transport cofactors that give the RCs their characteristic ability to convert light energy into chemical energy (*13*). This strongly suggests that Type-I and Type-II RCs both evolved from a universal ancestor that was likely a homodimer. The heterodimeric nature of these three RCs was due to gene duplications followed by divergence (*2*). Of the seven modern RCs described above, three still exist as homodimers. These are the GbRC, HbRC, and the reaction center of chloroacidobacteria. Improving our understanding of the structure and function of these still-homodimeric RCs is key in improving our understanding of the evolution of photosynthesis.

Heliobacteria

Heliobacteria are anaerobic photoheterotrophic organisms that were first identified by their unique pigment bacteriochlorophyll *g* (Bchl *g*) (*14*). They are the only organisms known to produce Bchl *g*, which is an isomer of Chl *a* at the 8^1 position (*15*).

Bacteriochlorophyll *g* is readily isomerized to Chl *a* upon exposure to oxygen and light, which may be the cause of oxygen sensitivity in these organisms ([15]). Another unique feature of heliobacteria is their lack of pigment binding antenna complexes ([16, 17]). All other known photosynthetic organisms utilize antenna complexes such as chlorosomes or phycobilisomes to aid in light harvesting. This, along with the homodimeric nature of the HbRC suggests it is one of the most primitive RCs still in existence.

Heliobacterial reaction center

The heliobacterial reaction center (HbRC) is a homodimeric Type-I RC that is widely considered the simplest RC ([18, 19]). The isolated HbRC consists only of two copies of PshA, which bind 22-45 Bchl *g* ([20, 21]). Each copy of PshA forms 11 transmembrane helices and has regions homologous to PsaA (and PsaB) of PSI, as well as CP43, the antenna subunit of PSII ([18, 22]). A bacterial ferredoxin subunit PshB, which is homologous to PsaC of PSI, associates with the core complex *in vivo*, however this peptide is lost during most isolation procedures ([20, 21, 23]). The isolated core complex has been shown to reduce soluble electron acceptors like flavodoxin even in the absence of PshB ([24]). There is currently debate on whether PshB is a subunit of the HbRC *in vivo* or just a tightly associating soluble electron acceptor.

While genetic studies on PshA of the HbRC described above suggest an evolutionary relationship to both PSI and PSII, current understanding of the HbRC function imply a much closer relationship to PSI. First, the primary acceptor (A_0) is a chlorophyll *a* as in all other Type-I RCs rather than a pheophytin as in Type-II RCs ([25]). Additionally, the HbRC uses Fe-S clusters as terminal electron acceptors, either in the form of PshB or F_X ([20, 21]). The 4Fe-4S cluster F_X is bound between the two copies of PshA (analogous to F_X in PSI) and acts as the terminal electron acceptor in the isolated HbRC core complex ([20, 21]). This will be further discussed in Chapter 5 below.

The mechanism of electron transfer in the HbRC resembles that of PSI described above with respect to the primary donor (P800), primary acceptor (A_0), and F_X. However
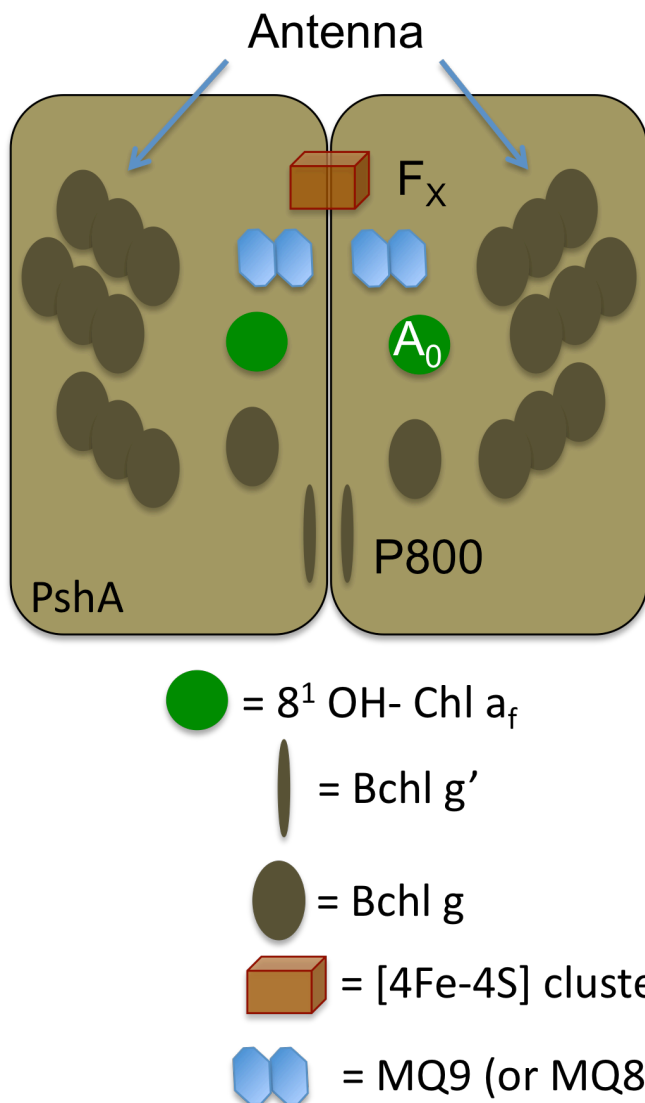
Figure 3. Cartoon representation of the proposed arrangement of cofactors in the HbRC. Conventional names for the electron transfer cofactors in the HbRC are labeled on the figure while the chemical identities of the various cofactors are shown in the legend. Structures for these cofactors can be found in Figure 5.

in the HbRC, there is no evidence that a semiquinone intermediate state is involved in electron transfer (*26, 27*). In fact, forward electron transfer from A_0 to F_X in the HbRC was not affected after the quinones were removed by solvent extraction (*28*). This is significant as an important distinction in the mechanisms of PSI and the PbRC discussed above is the function of the quinone. PSI binds two functionally identical quinones that serve as intermediates in one-electron transfer from A_0 to F_X. The PbRC binds two

functionally distinct quinones, one serving as a secondary electron acceptor similar to PhQ in PSI while the other serves as the terminal electron acceptor and becomes doubly reduced.

Despite the lack of an identified function, the isolated HbRC contains 1-2 quinones per RC (*21, 23*). Alternative functions have been proposed for these quinones, but these lack any experimental evidence in their support. One possibility is that the quinones function as a "safety valve" during periods of high electron flux through the RC. While this is an appealing possibility, as it would functionally link Type-I and Type-II RCs, no experiments have been designed to test this hypothesis directly.

CHAPTER 2: EXPERIMENTAL

Double reduction of plastoquinone in PSI

menD1 PSI samples

His-tagged PSI from *menD1* mutants of *Chlammydomonas reinherdtii* was provided by Dr. Mike McConnell.

Photoaccumulation

PSI samples containing 50 μg chlorophyll in 50 mM MES pH 5.5 with 0.03% βDDM were exposed to 64,000 saturating laser flashes from a frequency-doubled Nd:YAG laser (Continuum Electro-Optics, Inc.) in the presence of 10 mM sodium ascorbate and 1 μM PMS. Control samples were prepared in the dark with no exposure to laser flashes.

Cofactor analysis

Samples were concentrated 20-fold using Amicon Ultracel 50-kDa cutoff membranes, then extracted with 20 volumes acetone. Acetone extracts were evaporated to near dryness, and then resuspended in 5 volumes of methanol prior to injection of 200 μL of extract. Pigments and cofactors were eluted isocratically from a reverse-phase C-18 column (Ultrasphere 250 mm L x 4.6 mm ID packed with 5 μm particles) using a flow rate of 1.5 mL/min of a 17:1 mixture of methanol and hexane (*29*).   A JASCO MD-2018Plus PDA detector was used to monitor the absorbance of the eluent from 190-798 nm while a Perkin-Elmer LS55 fluorescence spectrophotometer was used to monitor emission at 320 nm with 290 nm excitation.

Characterization of purified HbRC

Isolation of and solubilization of membranes

HbRC samples were prepared essentially as described previously (*23*). All steps prior to membrane solubilization were performed under very low light in aerobic

conditions. Cells grown to mid-log phase were isolated by centrifugation for 10 minutes at 10,000 x g. Cell pellets were resuspended in 50 mM MOPS pH 7, then sonicated on ice for 14 minutes using cycles of 1 minute action and 4 minutes of rest. Unbroken cells were removed by centrifugation at 12,500 x g for 5 minutes. Membranes were pelleted by centrifugation at 200,000 x g for 1 hour, then resuspended to a bacteriochlorophyll g concentration of 0.5 mM. Membranes were solubilized in the dark under anaerobic conditions by adding βDDM to a final concentration of 0.9% (w/v) and stirring on ice for 1 hour. Insoluble material was removed by centrifugation at 200,000 x g for 30 minutes.

Purification of HbRC

Solubilized membranes were passed through a DEAE-cellulose anion exchange column (Whatman DE52) that was equilibrated with 50 mM MOPS pH 7 with 0.02% βDDM in the dark under anaerobic conditions. The brown-colored flow-through was collected and loaded onto a CM-sepharose (Sigma) column that was equilibrated with 50 mM MOPS pH 7 with 0.02% βDDM. The brown band that contained the HbRC was washed with 3 column volumes 50 mM MOPS pH 7 with 0.02% βDDM, then 1 column volume 50 mM MOPS pH 7 with 0.02% βDDM and 10 mM $MgSO_4$. The bound HbRC was eluted with buffer 50 mM MOPS pH 7 with 0.02% βDDM containing 100 mM $MgSO_4$.

Pigment composition of HbRC

HbRC samples prepared by Dr. Iosifina Sarrou were extracted with 10-50 volumes acetone and incubated on ice for 5 minutes (*25*). Extracts were passed through a 0.2 μm filter prior to injection of 200 μL onto a reverse-phase C-18 column (Ultrasphere 200 mm L x 4.6 mm ID packed with 5 μm particles).   Pigment separation was achieved as described previously using a flow rate of 1 mL/min (*30*). A JASCO MD-2018Plus PDA detector was used to monitor the absorbance of the eluent from 190-798 nm. Peaks were collected under argon in the dark and prepared as described previously using non-

acidic matrices to prevent damage to pigments (*31*). Samples were analyzed using an

Applied Biosystems DE-STR MALDI-TOF mass spectrometer.

Quinone content of HbRC

Quinones were extracted using two methods that produced similar results. The

first method involved extraction with acetone as described above (*25*). The second

method involved an initial extraction using acetone and methanol. The initial extract was

then extracted with petroleum ether and evaporated to dryness. Extracted pigments and

cofactors were resuspended in acetone prior to injection of 200 μL of extract onto a

reverse-phase C-18 column. Pigments and cofactors were eluted isocratically using a

flow rate of 1.5 mL/min of a 4:1 mixture of methanol and isopropanol (*32*).

Characterization of F_X in the HbRC

HbRC samples

HbRC isolated as described above was concentrated to a bacteriochlorophyll g

concentration of 3 mM for EPR measurements, 1 mM for protein-film voltammetry

measurements, 1 μM for measurements on the JTS or with single-photon counting, or

60 μM for ultrafast transient absorption measurements.

Carbonate-washed membrane samples

Carbonate-washed membrane samples were prepared essentially as described

previously (*33*). Membranes isolated as described above were resuspended to an

OD788 of 1-2 in 100 mM sodium carbonate pH 11.5 buffer and incubated for 1 hour in

the dark under anaerobic conditions. Following incubation, membranes were harvested

by centrifugation at 45,000 RPM for 1 hour. Membrane pellets were again resuspended

in 100 mM sodium carbonate pH 11.5 buffer for an additional hour before being

harvested by centrifugation at 45,000 RPM for 1 hour. Pellets were resuspended in

50 mM MES pH 6 with 20 mM MgSO$_4$ for all experiments unless otherwise noted.

Samples were resuspended to a bacteriochlorophyll g concentration of approximately 3

mM for EPR experiments or approximately 1 μM for optical measurements.

Millisecond timescale pump-probe spectroscopy

Pump-probe spectroscopy on the millisecond timescale was performed on a JTS-

10 kinetic spectrophotometer (BioLogic) with a frequency-doubled Nd:YAG

laser (Continuum Electro-Optics, Inc.) as the actinic source and an 800 nm LED as the

probe source. Samples were excited with a 6 ns saturating laser pulse at 532 nm, then

probed with low-intensity 10-μs flashes from the 800 nm LED beginning 500 μs after the

laser flash.

Ultrafast transient absorption

Picosecond transient absorption measurements were performed using a broad

band pump-probe setup described previously by Dr. Su Lin (*34*). Laser pulses of 100 fs

duration at 800 nm were generated from a regenerative amplifier system at a repetition

rate of 1 kilohertz (Tsunami and Spitfire, Spectra-Physics). Part of the pulse energy was

used to pump an optical parametric amplifier (IR OPA, Spectra-Physics) to generate 575-

nm excitation pulses. The broad-band probe pulse was generated by focusing a weak

800-nm beam into a 3-mm sapphire plate, and sent to an optical compressor composed

of a pair of prisms, before it was focused onto the sample. The white-light probe pulses

were then dispersed by a spectrograph and detected using a CCD camera (DU420,

Andor Technology). The collected data had a ~2.3 nm spectral resolution. The

polarization of the pump pulses was set to the magic angle (54.7°) with respect to that of

the probe pulses. Samples were loaded into a spinning wheel with an optical path-length

of 1.2 mm for the ascorbate-reduced samples or a sealed quartz cuvette with an optical

path-length of 2 mm for dithionite-reduced samples. The optical density of the sample at

788 nm was adjusted to 1.5 in the 2 mm path-length.

Decay-associated spectra were calculated from global fitting, accounting for deconvolution of the recorded signals with instrument response function using locally written software, ASUFIT (http://www.public.asu.edu/~laserweb/asufit/asufit.html).

Time-correlated single-photon counting

Fluorescence decay kinetics was measured using the time-correlated single-photon counting (TC-SPC) technique. The excitation source was a fiber supercontinuum laser based on a passive modelocked fiber laser and a high-nonlinearity photonic crystal fiber supercontinuum generator (Fianium SC450). The laser provides 6-ps pulses at a repetition rate variable between 0.1 – 40 MHz. The repetition rate was 10 MHz unless otherwise noted. The laser output was sent through an Acousto-Optical Tunable Filer (Fianium AOTF) to obtain excitation pulses at desired wavelength of 575 nm. Fluorescence emission was collected at 90° and detected using a double-grating monochromator (Jobin-Yvon, Gemini-180) and a microchannel plate photomultiplier tube (Hamamatsu R3809U-50). The polarization of the emission was 54.7° relative to that of the excitation. Data acquisition was done using a single-photon counting card (Becker-Hickl, SPC-830). The IRF had a FWHM of 50 ps, measured from the scattering of sample at the excitation wavelength. The data was fitted with a sum of exponential decay model using ASUFIT.

Preparation of EPR samples

Dithionite-reduced samples were treated with 10 mM dithionite for optical measurements or 30 mM dithionite for EPR measurements for 30 minutes in the dark. Illumination of EPR samples was performed using a 1000 W Oriel quartz-tungsten halogen lamp (Model 6405) passed through a copper sulfate solution to give a light intensity of 750 $\mu E/m^2/s$ at room temperature for 30 seconds. Following illumination, samples were given a 2 second period of darkness prior to freezing in a dry ice ethanol bath. Samples were stored in the dark in liquid nitrogen prior to measurement.

EPR measurements

Measurements were performed with a Bruker E580 X-band spectrometer (Bruker, Silberstreifen, Germany) with an Oxford Model 900 EPL liquid helium cryostat (Oxford Instruments, Oxfordshire, UK). All spectra were measured with a modulation frequency of 100 kHz and modulation amplitude of 1 mT. The microwave power used was 0.25 mW with a frequency of approximately 9.43 GHz unless otherwise noted.

Pulse experiments were recorded at 4 K using a Bruker ELEXSYS E580 FT−EPR X-band spectrometer equipped with a dielectric ring resonator (ER 4118X-MD5). The three-pulse ESEEM ($\pi/2- \tau-\pi/2-t-\pi/2-\tau-$echo) experiments were performed with a separation of the first and second microwave pulses of 144 ns and a $\pi/2$ pulse length of 8 ns. In total, 220 data points were recorded in the ESEEM experiments. The microwave frequency was 9.68 GHz, the time increment of the t time was 8 ns, and the shot repetition time was 259 μs. The resulting modulation pattern was baseline-corrected, a Hamming window function was used for apodization, and the array was increased to 512 points by zero-filling prior to transformation into the frequency domain with Fourier analysis. The ESEEM spectrum shown in this work is a magnitude spectrum. No dead time reconstruction procedures were used. The phase-memory time (T2*) was measured by the Hahn echo decay method.

Fitting of EPR spectra

Fitting of EPR spectra was performed using EasySpin (version 3.0.0) by Dr. Marco Flores (*35*). The fitting parameters used were the three g values (g_x, g_y, and g_z), the line width (ΔB), and the zero-field splitting parameters (D and E). The fitting method used here was similar to those previously described by Flores *et al.* (*36*).

Thin film voltammetry

Glassy carbon (GC) electrodes (3 mm diameter, BASi) with a DMPC/HbRC monolayer were prepared by Dr. Idan Ashur as follows. A 3 mM DMPC solution was

prepared by sonicating in 50 mM Tris buffer pH 8.3. Sonication of the mixture for 4 hours

yielded a clear solution suitable for electrochemical measurements. Equal volumes of

the 3 mM DMPC and HbRC solutions were mixed and a 5 mL aliquot of the mixture was

incubated on the clean GC overnight at 4 °C. The electrochemical measurements were

performed using a CV50W (BASi) potentiostat with a three-electrode setup. The

reference electrode was Ag/AgCl (BASi), and a platinum wire served as the counter

electrode. The electrochemical cell was filled with 5 ml of the working buffer (50 mM,

0.1 M NaCl Tris buffer pH 8.3) and purged for 25 minutes with N_2 gas. The

HbRC/DMPC/GC working electrode was rinsed with the working buffer in order to remove

loosely bound proteins and was placed in the electrochemical cell. An additional

10 minutes of N_2 purging were applied prior to measuring. During data collection, the N_2

tube was placed slightly on top of the solution to maintain anaerobic conditions

throughout the measurement. The stability of the pH value in the cell was assessed

before and after each measurement using a 2 mm pH electrode (HI1093, HANNA

Instruments).

Spectroelectrochemistry

　　　　HbRC samples were prepared in buffers ranging from pH 6-10 in the presence of

10 mM ascorbate and 0.02% βDDM. MES was used for pH 6-6.5, MOPS was used for

pH 6.6-7.9, Tricine was used for pH 8-8.9, and Glycine was used for pH 9-10. Laser-

flash induced photobleaching was measured at 800 nm on the JTS. The samples were

then treated with 10 mM dithionite in the dark for up to 3 hours. Photobleaching

measurements were taken every 15 minutes until the amplitude of the bleaching at

500 μs after the flash remained constant between measurements. The fraction reduced

was calculated by dividing the amplitude of the bleaching for the dithionite treated sample

by the amplitude measured prior to addition of dithionite. The ambient reduction potential

of the various solutions were measured in the absence of the HbRC with 50 μM of methyl

viologen, benzyl viologen, triquat, and dimethyl triquat using a saturated calomel electrode and platinum counter-electrode

Double reduction of MQ by the HbRC

Sample preparation

HbRC were prepared at 1 μM Bchl *g* and subjected to various light and chemical treatments as discussed below. Heliobacterial membrane samples were prepared at 10 μM Bchl *g* and subjected to various light and chemical treatments as discussed below Following treatments, HbRC samples were concentrated 20-fold and extracted in 80% acetone. For samples treated with dithionite, the concentrated sample was diluted 5 fold in buffer without dithionite and re-concentrated. This was repeated a total of 10 times so that the final concentration of dithionite in the extracted sample was less than 1 nM. This procedure should minimize artifactual reduction of the extracted quinones by dithionite. Membrane samples (100 μL) were directly extracted following photoaccumulation with 500 μL acetone to minimize oxidation of menaquinol.

Cofactor analysis

Pigments and cofactors were eluted isocratically from a reverse-phase C-18 column (Phenosphere 250 mm L x 4.6 mm ID packed with 5 μm particles) using a flow rate of 1.5 mL/min of a 17:1 mixture of methanol and hexane.   A JASCO MD-2018Plus PDA detector was used to monitor the absorbance of the eluent from 190-798 nm.

Photoaccumulation conditions

Samples were photoaccumulated as described above for PSI samples with the exception that 5,000 saturating flashes were used unless otherwise noted.

CHAPTER 3. DOUBLE REDUCTION OF PLASTOQUINONE IN PHOTOSYSTEM I

Background

Unlike Type-II RCs, the semiquinone in PSI does not become doubly reduced under normal conditions. The protein environment surrounding PhQ (A_1) in PSI destabilizes the semiquinone state giving it an abnormally low reduction potential and a very short lifetime (*37*). Double reduction of PhQ in PSI has been shown *in vitro*, but requires strongly reducing conditions (*38, 39*). To study double reduction of quinones in PSI under more physiological conditions, the native PhQ must be replaced with alternative quinones.

In previous studies, PhQ in the A_1 binding pocket of PSI has been replaced by extraction followed by addition of alternative quinones (*40, 41*). This procedure requires harsh treatment with organic solvents that leads to loss of antenna chlorophylls. More recently, PSI lacking PhQ has been isolated from cyanobacteria and green algae using mutations in the PhQ biosynthetic pathway (*42*). The PSI isolated from these *menA, menB,* and *menD* mutants incorporates plastoquinone (PQ) in the A_1 binding pocket. PQ, with a reduction potential of 100 mV, should be more easily reduced in the A_1 binding pocket than PhQ (-70 mV) (*13*). Additionally, the lifetime of the semiquinone radical is significantly increased in these mutants (*43*). These properties make PSI isolated from *menD1* mutants of *C. reinhardtii* ideal for the study of double reduction of quinones by PSI.

HPLC analysis of photoaccumulated menD1 PSI

Previous studies on the redox state of PQ in photosynthetic organisms have used RP-HPLC to separate the oxidized form (PQ) from the doubly reduced form (PQH_2) (*29*). The addition of two O-H bonds to the quinone head group increases the polarity and decreases the retention time of PQH_2 on a C-18 column. While PQ is easily detectible by its absorbance at 260 nm, PQH_2 has a much weaker spectroscopic signature and often requires more sensitive techniques for detection. Fluorescence

16

emission at 330 nm with 290 nm excitation has been utilized in previous studies and was

used here to detect and quantify PQH_2.

The A_{260} chromatogram from the extracts of dark-treated *menD1* PSI in Figure

4A shows a peak at a retention time of 35 minutes. This is identified as PQ by both

retention time and spectral properties as compared to a PQ standard. By comparing the

area of the PQ peak with the area of the chlorophyll *a* peak and using published

extinction coefficients, it is possible to determine the relative levels of PQ in the *menD1*

PSI samples. The dark-treated *menD1* PSI samples show a PQ:Chl a ratio of 1:193. In

the extracts of the *menD1* PSI subjected to 64,000 saturating laser flashes, the PQ peak

is below the limit of detection with this system (Figure 4B). However, a new peak in the
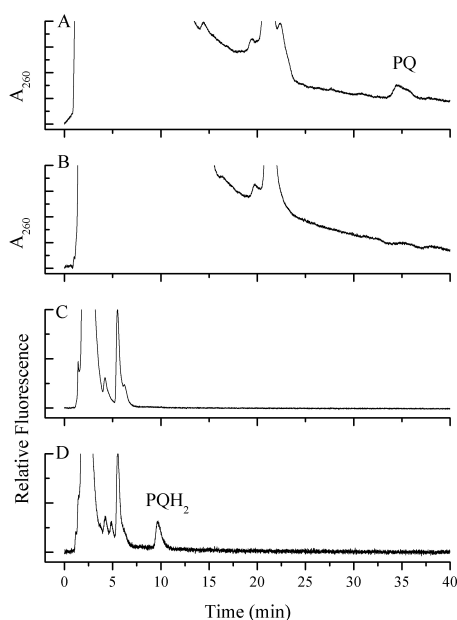
Figure 4. Pigments extracted from *menD1* PS1 particles following dark incubation (A and C) or photoinactivation (B and D) were subjected to reverse-phase HPLC. Chromatograms monitored absorbance at 260 nm (A and B) or fluorescence emission at 330 nm using excitation at 290 nm (C and D). The PQ and PQH_2 labels indicate the elution times of those species, as determined using PQ-9 and PQH_2-9 standards, respectively (not shown). Reprinted with permission from McConnell, MD., Cowgill, JB., Baker, PL, Rappaport, F, and Redding, KE (2011) Double Reduction of Plastoquinone to Plastoquinol in Photosystem 1. *Biochemistry* 50:11034-11046. Copyright 2012 American Chemical Society.

fluorescence emission chromatogram in Figure 4D appeared with a retention time of

10 minutes. This was identified as PQH_2 by comparison to the PQH_2 standard that had

been made by reducing PQ with KBH_4. The level of PQH_2 in the extract was quantified

by comparison of the fluorescence emission peak to a standard curve prepared using the

reduced PQ standard. Comparison of the PQH_2 concentration determined using this

method to the concentration of chlorophyll a injected gives a PQH_2:Chl a ratio of 1:250.

Discussion

The content PQ in *menD1* PSI is similar to the content of the native PhQ in wild-

type PSI in *C. reinhardtii*, with quinone to chlorophyll a ratios of 1:193 and 1:150,

respectively (*44*). This suggests that the majority of A_1 binding sites are occupied by PQ

After 64,000 laser flashes in the presence of PMS and ascorbate, PQ is no longer

detectable in the extracts of *menD1* PSI. The loss of the PQ peak is accompanied by the

rise of a PQH_2 peak that is present at a ratio of 1 PQH_2 to 250 chlorophyll *a*. This

suggests that ~75% of the PQ in the *menD1* PSI samples is converted to PQH_2 following

photoaccumulation. This is in agreement with levels of photoinactivation of PSI

determined by pump-probe spectroscopy (*45*). Thus, PSI can doubly reduce PQ in the

A_1 binding site under mildly reducing conditions.

The A_1 binding site evolved to destabilize the semiquinone state and reduce its

lifetime. A tryptophan residue π-stacks with the aromatic rings of the quinone (*46*). This

hydrophobic interaction destabilizes any accumulation of charge on the quinone head-

group. Furthermore, the very hydrophobic environment of the A_1 site minimizes the risk

of protonation of the reduced states of the quinone, preventing formation of the stable

hydroquinone state. Because the double reduction of PQ in *menD1* PSI is pH

dependent, such proton transfer reactions are likely a rate-limiting step (*45*). These

features make double reduction of quinones in the A_1 site very difficult. This activity is

not physiologically relevant, as it requires use of strongly reducing conditions imposed by

dithionite at high pH or replacement of the native quinone. The ability of PSI to doubly

reduce quinones may be a vestigial feature that hints at an activity once possessed in

ancestral forms. This will be further discussed in Chapter 7.

CHAPTER 4. CHARACTERIZATION OF PURIFIED HBRC

Background

Current estimates on the antenna size of the HbRC range from 22 to 45 Bchl g per RC ([20, 21]). The large discrepancy in the antenna size determined in previous studies is due to different methods of determining the concentration of HbRC in solution. Many of these studies normalize the Bchl g concentration (determined by absorbance at the Q_y maximum) to the concentration of P800 determined using differential extinction coefficients. However, the differential extinction coefficients used range from 100-200 mM^{-1} ([21]). In the most recent study, the Bchl g concentration was normalized to the concentration of non-heme iron (assuming 4 irons per RC) and produced a ratio of 22 Bchl g per HbRC ([20]).
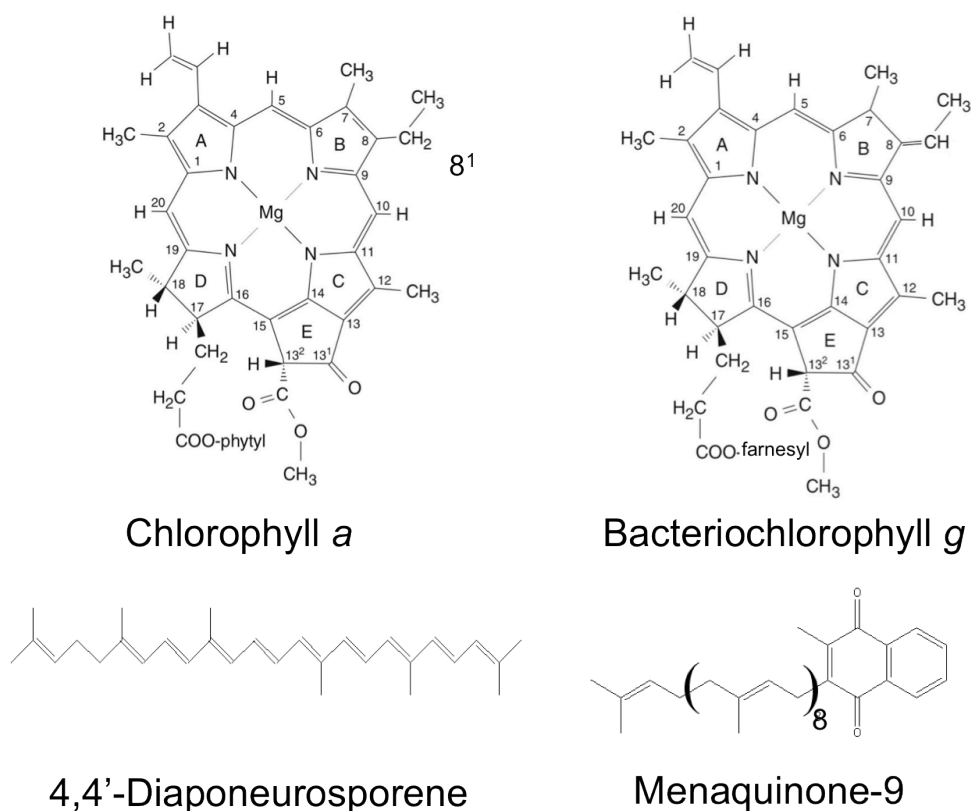
Figure 5. Chemical structure of relevant pigments and cofactors. Bchl g' has an identical structure to Bchl g with different stereochemistry at the 13^2 position. The primary acceptor of the HbRC, 8^1-OH Chl a_f has a similar structure as Chl a with the exception that it has a hydroxyl group added at the 8^1 position and the tail is a farnesyl group rather than the phytyl group shown.

The approaches described above provide estimations of the total Bchl g content of the HbRC, but do not allow quantification of the other pigments and cofactors present. In addition to the major pigment Bchl g, the HbRC also contains Bchl g', 8^1-OH-Chl a_F, 4,4'-diaponeurosporene, and MQ (19). Previous studies have shown that there are two Bchl g' and two 8^1-OH-Chl a_F per RC, which are believed to form the primary donor (P800) and primary acceptor (A_0), respectively (25, 47). Therefore, the concentrations of Bchl g' and 8^1-OH-Chl a_F may be used as internal standards for quantification of the Bchl g antenna size as well as quinone and carotenoids content of the HbRC. RP-HPLC will be used in this study to allow separation and quantification of the major pigments and cofactors of the HbRC. The chemical structures of the cofactors bound by the HbRC are shown in Figure 5.

Pigment composition

The acetone extracts of the purified HbRC show 4 major peaks when subjected to RP-HPLC as shown in Figure 6A. Based on their absorbance spectra (Figure 6C) and MALDI-TOF determined masses, peaks 1-4 can be assigned to 8^1-OH-Chl a_F Bchl g, Bchl g', and 4,4' diaponeurosporene, respectively. While Bchl g and Bchl g' have identical masses and spectra, peak 2 is identified as Bchl g based on its increase abundance compared with peak 3. After correcting peak areas using published extinction coefficients, the ratios of each of these pigments in the extracts were determined. Figure 4B shows the pigment composition of the HbRC based on either two Bchl g' or two 8^1-OH-Chl a_F RC. As expected, both methods give similar results of approximately 20 Bchl g, two Bchl g', two 8^1-OH-Chl a_F, and one 4,4'-diaponeurosporene per HbRC. This gives an estimated antenna size of 22 total Bchl g (Bchl g + Bchl g'), which is consistent with the most recent estimates (20).
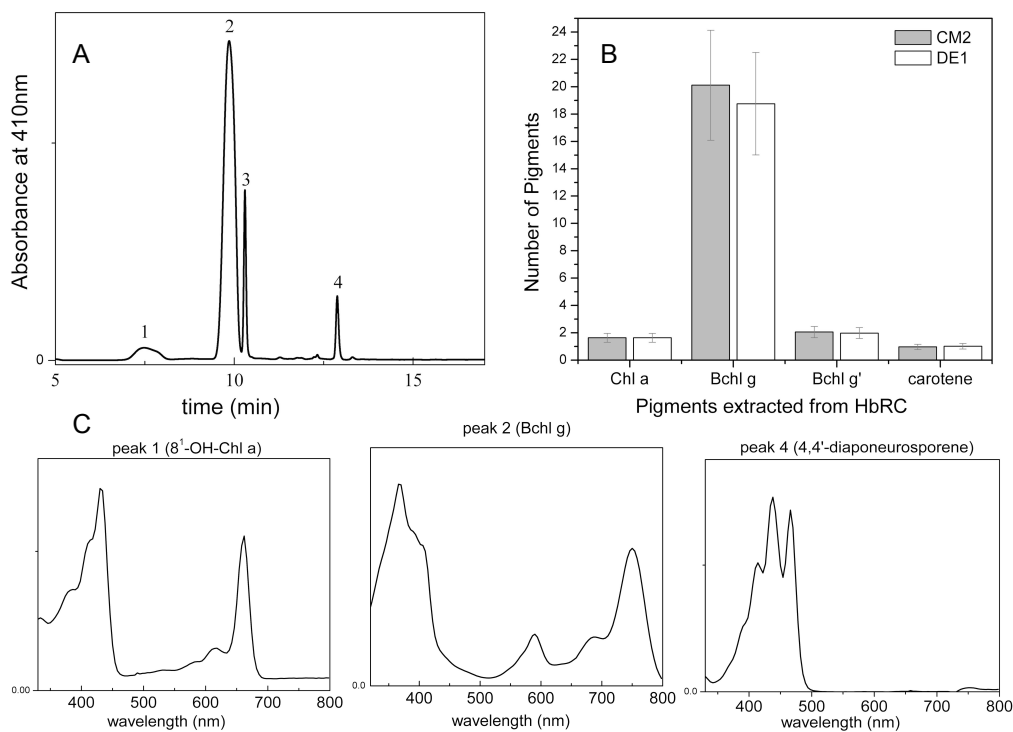
Figure 6. Analysis of the pigments associated with the HbRC. A: Representative HPLC chromatogram (at 410 nm) of an acetone extract of HbRC fraction CM-20. Peak 1 is due to pigments related to Chl a (Chl a_F and 8^1-OH-Chl a_F), while peaks 2 and 3 are BChl g and BChl g', respectively; peak 4 is 4,4'-diaponeurosporene. B: Estimated number of pigments per HbRC by integration of peak areas of separated pigments at their absorption maximum. The extinction coefficients used for the BChl g (and g') and Chl a was 76 mM^{-1} cm^{-1}, and 150 mM^{-1} cm^{-1} was used for the carotenoid. The histogram shows the number of pigments calculated for DS-FT and CM-20 fractions (see text for details). C: Absorption spectra of the pigments in peaks 1, 2 and 4 (8^1-OH-Chl a_F, BChl g, and 4,4'-diaponeurosporene, respectively). This figure is reprinted from Springer and the original publisher/ *Photosynthesis Research*, 111, 2012, 291-302, Purification of the photosynthetic reaction center from *Heliobacterium modesticaldum*, Sarrou, I., Khan, Z., Cowgill, J., Lin, S., Brune, D., Romberger, S., Golbeck, J. H., Redding, K. E., Figure 2, with kind permission from Springer Science and Business Media.

Quinone Content

A separate HPLC method was used to identify and quantify the quinones in the isolated HbRC (Figure 7). In this method, two peaks were identified as quinones by the absorption spectra (Peaks 2 and 3). Peak 3 was identified as MQ9 by coelution the MQ9
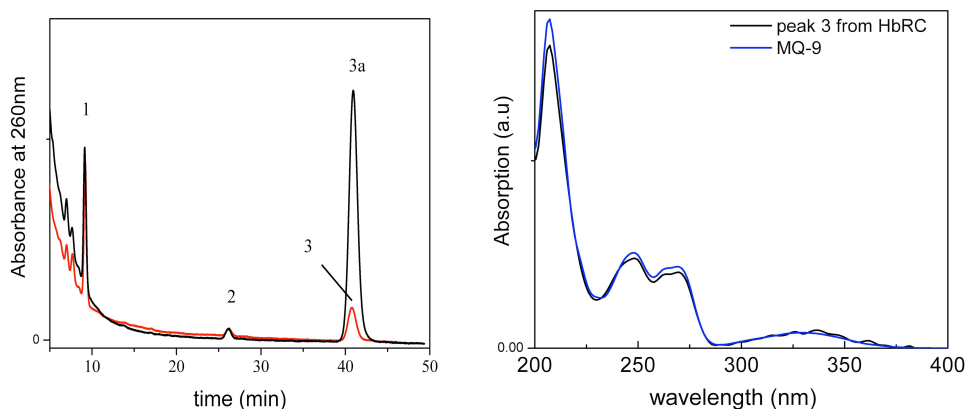
Figure 7. Identification and quantification of the quinone in the HbRC. A: Representative HPLC chromatogram (at 260 nm) of an extract from HbRC without (red) or with (black) the addition of 10 µg/mL MQ-9. Peak 1 is due to 4,4'-diaponeurosporene; peaks 2 and 3 are MQ-8 and MQ-9, respectively. B: Absorption spectra of peak 3 (black) and an authentic MQ-9 sample (blue). The intensities of the two spectra were normalized for comparison. This figure is reprinted from Springer and the original publisher/ *Photosynthesis Research*, 111, 2012, 291-302, Purification of the photosynthetic reaction center from *Heliobacterium modesticaldum*, Sarrou, I., Khan, Z., Cowgill, J., Lin, S., Brune, D., Romberger, S., Golbeck, J. H., Redding, K. E., Figure 3, with kind permission from Springer Science and Business Media.
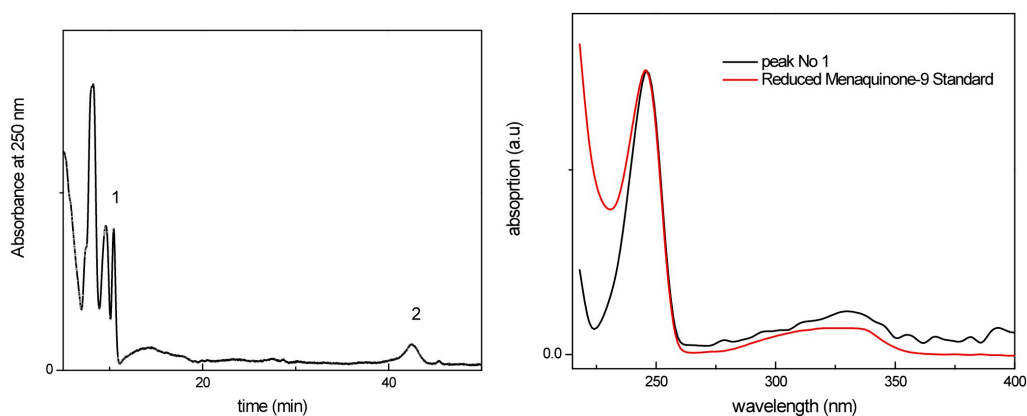
Figure 8. HPLC analysis of quinones in membranes from *H. modesticaldum.* Solvent extracts from membranes were analyzed by HPLC using the same method as in Figure 5. **A:** HPLC chromatogram of extracted pigments at 250 nm. Peak 1 is MQH_2 and peak 2 is MQ-9. HPLC method was the same as used in Figure 7. **B:** UV-visible absorption spectra of peak 1 and MQH_2 (made by reducing MQ-9 with $NaBH_4$). This figure is reprinted from Springer and the original publisher/ *Photosynthesis Research*, 111, 2012, 291-302, Purification of the photosynthetic reaction center from *Heliobacterium modesticaldum*, Sarrou, I., Khan, Z., Cowgill, J., Lin, S., Brune, D., Romberger, S., Golbeck, J. H., Redding, K. E., Figure S5, with kind permission from Springer Science and Business Media.

standard. Peak 2 most likely corresponds to MQ8, which has an identical head group to MQ9, but the hydrophobic tail is shorter by one isoprenoid unit. The quinones were quantified by comparison of the peak areas to the peak area for 4,4'-diaponeurosporene (Peak 1) after correction using published extinction coefficients for MQ and 4,4'-diaponeurosporene. Quantification by this method yields a quinone content of 1.5-1.6 MQ per HbRC, which is consistent with previous reports on HbRC isolated from *H. mobilis* (*21*)*.

Additionally, the quinone content of membrane samples was determined via RP-HPLC (Figure 8). In membranes, there is a mixture of MQ8, MQ9, and MQH$_2$, the reduced form of MQ. The oxidized and reduced forms are present in approximately equal abundance at a ratio of about 4 or 5 quinones per HbRC. This is similar to previous reports on the quinone content of membranes from *H. mobilis*, though the redox state of these quinones was not investigated in this species (*21*).

The quinone and carotenoid content of HbRC samples prepared on a larger scale was found to be more variable as summarized in Table 1. These samples show an average of 0.75 quinones and 0.41 carotenoids per HbRC as compared to ~1.6 quinones and 1 carotenoid per reaction center that was determined in the analysis above. This discrepancy may arise due to changes to the HbRC isolation protocol designed to accommodate larger scale preparations for measurements such as EPR. Use of larger columns and more extensive washing on the column may cause labile cofactors to be washed out of the immobilized HbRC. This suggests that both the quinones and the carotenoids bound by the HbRC may be more labile than previously thought.

Table 1: Quinone and carotenoid content of large-scale HbRC preparations.

	Small-scale preparation	Large-scale preparations				
4,4'-diaponeurosporene	1.20	0.52	0.46	0.19	0.46	0.44
MQ	1.70	0.75	0.41	1.2	0.70	0.69

*All values are normalized to 22 total Bchl g per reaction center (Bchl g + Bchl g')

24

Discussion

   The antenna size of 22 Bchl g per HbRC is consistent with the most recent

estimate based on normalization to 4 non-heme irons per RC (*20*). This is a very small

antenna size relative to Photosystem I, which binds over 90 Chlorophyll a and an

additional 20+ carotenoids per RC. The large difference in the antenna size between PSI

and the HbRC is surprising given the similar topology of the core dimers that are

responsible for binding the majority of the pigments. The core polypeptide of the HbRC

(PshA) is comprised of 11 hydrophobic regions that are believed to form transmembrane

α-helices similar to the PsaA/PsaB core polypeptides of PSI (*3, 48*).

   Another surprising find is that there is only one carotenoid bound by the isolated

HbRC. Given the perfect symmetry of the HbRC predicted by the presence of a single

core polypeptide in the genome, each cofactor should be present in an even

stoichiometry. One possible exception is cofactors like F_X that are bound at the

symmetry axis between the copies of the homodimer. While this cannot be ruled out until

the X-ray structure of the HbRC is determined, a more likely explanation is that the

carotenoid is susceptible to being "washed out" during the isolation procedure, as

suggested by the variability of the carotenoid content in the HbRC samples prepared on a

larger scale with more extensive column washing.

   The quinone quantification described here shows that 1-2 quinones are present

in the isolated HbRC while membranes have 4-5 quinones per RC. All quinones in the

isolated HbRC are in the oxidized form while the reduced and oxidized forms are present

in approximately equal abundance in anaerobically isolated membranes. The main

quinone is MQ9, though MQ8 was found at about a 1:6 ratio to MQ9 for both membrane

and HbRC samples. This is consistent to reports on the quinone content of the HbRC

and membranes isolated from *H. mobilis* (*21*). Despite the presence of quinones in these

samples, no EPR signal attributable to a semiquinone could be generated by

photoaccumulation (*23*). The role of the quinone in these RCs will be further investigated

in Chapter 6.

CHAPTER 5. CHARACTERIZATION OF FX IN THE HBRC

Background

Iron-sulfur clusters are ubiquitous in biology, with functions ranging from redox cofactors to oxygen sensors. They also serve as the terminal electron acceptors in Type-I RCs. These iron-sulfur clusters are among the lowest potential cofactors found in biology and are the starting point for many important reactions in anabolic metabolism such as the reduction of $NADP^+$ to NADPH.

In the isolated HbRC, the 4Fe-4S cluster F_X serves as the terminal electron acceptor (*20, 21*). The binding site for F_X is located at the symmetry axis between two copies of the PshA homodimer. This region of the PshA peptide is the area of highest conservation between the HbRC and Photosystem I with 75% sequence identity over a 12 amino acid range (*18*). There are many complicating factors that have limited studies on F_X in both PSI and the HbRC. First, the low potential and highly buried nature of F_X makes it difficult to reduce for investigations by techniques such as EPR. Additionally, the fast spin-spin relaxation properties of the clusters make it difficult to detect even at liquid helium temperatures. Finally, the optical signatures of the cluster are much weaker than those of the chlorin radicals generated during charge separation, making detection by transient absorption difficult.

Despite these complications, several studies have examined the spectroscopic properties of F_X in the HbRC. The earliest studies used light-minus-dark difference spectra in the visible region to show a species with a broad absorption maximum around 430 nm, which is characteristic of a reduced Fe-S cluster (*49*). Recently, two studies have reported different EPR spectra that were both attributed to F_X (*20, 50*). In the first, membrane samples that were pre-reduced with dithionite were measured under illumination at 5 K to generate light-minus-dark difference spectra by CW as well as transient EPR. The corresponding signal was attributed to F_X in a S=1/2 state with similar g-values to those reported for F_X in PSI (*50*). However, this signal was not observed under similar conditions with the isolated HbRC. The next study illuminated the

26

HbRC at room temperature in the presence of dithionite prior to freezing. This generates

a signal which was attributed to F_X in a S=3/2 state, similar to a signal observed for the

4Fe-4S cluster of the reduced nitrogenase Fe protein (*20*).

Given the controversy surrounding the spectroscopic properties of F_X in the

HbRC, three new ways were developed to generate EPR signals that can be attributed to

F_X^-. Additionally, thin film voltammetry and spectroelectrochemistry were used to

determine the electrochemical properties of F_X in the isolated HbRC.

Direct reduction of Fx by dithionite

The ascorbate reduced HbRC shows laser flash-induced photobleaching at

800 nm that recovers by monoexponential decay with a $t_{1/2}$ of 14 ms. This has previously

been identified as charge recombination of the $P800^+$-F_X- state (*20*). Following treatment

of this sample with 10 mM dithionite at pH 10 for 30 minutes in the dark, less than 5% of

the flash-induced photobleaching remains. Over 99% of the signal is recovered when

this sample is exposed to oxygen for 2 minutes. This suggests that dithionite causes

light-independent reduction of a cofactor of the HbRC that blocks electron transfer to F_X

and is reversible by oxygen exposure.
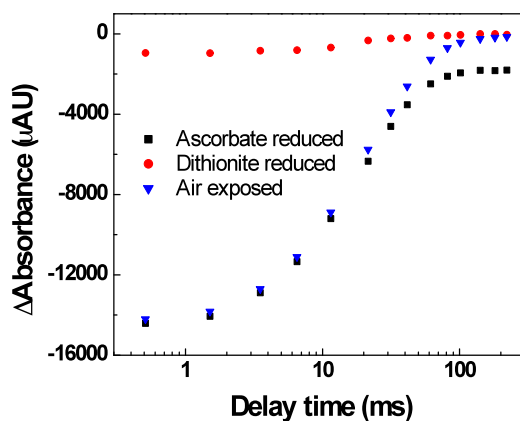
Figure 9. Charge recombination kinetics in the HbRC reduced with ascorbate (squares) and dithionite (circles) plotted on a logarithmic timescale. The dithionite-reduced sample was exposed to air for 2 minutes prior to recording the "air exposed" trace (triangles). A 6 ns saturating laser pulse at 532 nm was used as the excitation source while an 810 nm LED was used to probe changes in sample absorbance starting 500 μs after the flash.

Millisecond-timescale pump-probe spectroscopy does not have the resolution required to study the dithionite-reduced HbRC, so picosecond scale transient absorption spectroscopy was used. Because the only chlorophyll a in the HbRC are bound at the A_0 positions, the electron transfer kinetics of A_0 can be directly studied using the transient absorption kinetics in the red region on the picosecond to nanosecond timescale (*25*).

Global analysis of the transient absorption kinetics from 640-720 nm for the ascorbate reduced HbRC shown in Figure 10A identifies four components with exponential lifetimes of 3 ps, 25 ps, 725 ps, and a component that does not decay on the 4-ns timescale of the measurement. The decay-associated spectra for the 3- and 25-ps components show a broad increase in absorption with peaks between 670 nm and 680 nm. The broad absorption increase and short lifetime of the 3-ps component is characteristic of energy redistribution within the antenna pigments. The 25-ps component corresponds to the trapping time of the HbRC that can be attributed to excited-state absorption of antenna Bchl g. Decay of the excited antenna Bchl g corresponds to the
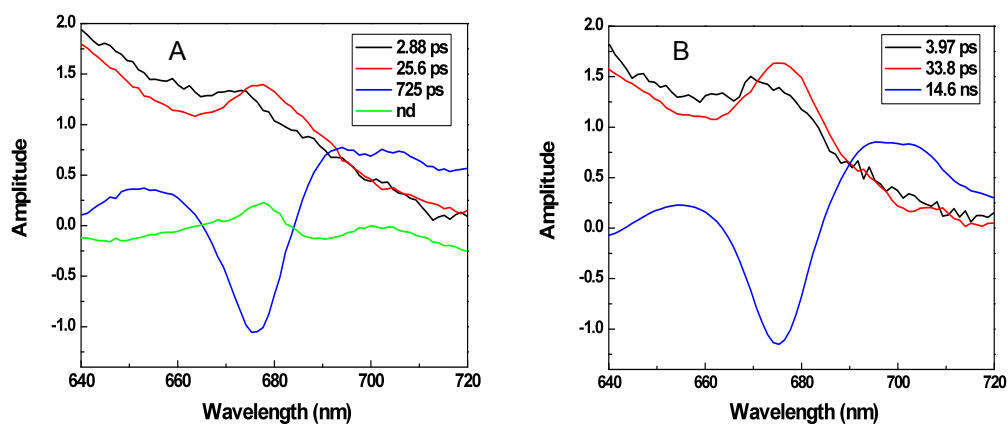
Figure 10. Decay-associated spectra from global analysis of the transient absorption of HbRC samples in the red region. Samples were reduced with either 10 mM ascorbate and 20 μM PMS (left) or 10 mM dithionite (right).The data was fit using global analysis with a sum of 4 exponentials for the ascorbate reduced HbRC and 3 exponentials for the dithionite-reduced HbRC. Samples were excited at 575 nm at a frequency of 1 kHz.

formation of the $P800^{+}$-A_0^{-} state (*23*). The 725-ps component in Figure 9 shows bleaching centered at 675 nm that is characteristic of $P800^{+}$-A_0^{-} state, which decays due to forward electron transfer to F_X (*27*). The non-decaying component shows a decay-associated spectrum that is characteristic of an electrochromic bandshift of A_0 caused by the nearby charge of $P800^{+}$.

Global analysis of the dithionite-reduced HbRC shown in Figure 10B identifies three components with exponential lifetimes of 4 ps, 33 ps, and 14.6 ns. The lifetimes and decay associated spectrum of the 4-and 33-ps components suggest that energy trapping by the HbRC may be slightly altered by dithionite treatment, though this is not the focus of these measurements. The 14.6-ns component in the dithionite-reduced HbRC is nearly identical to the 725 ps component in the ascorbate reduced HbRC. This suggests that the $P800^{+}$-A_0^{-} state decays with a lifetime of 14.6 ns rather that the ~700-ps decay expected due to forward electron transfer to F_X. This indicates that electron transfer from A_0 to F_X is blocked as suggested by the millisecond pump-probe measurements. The increased lifetime of the $P800^{+}$-A_0^{-} state can clearly be seen in the 675 nm transient absorption kinetics in Figure 11. Additionally, there is a small recovery in 675 nm bleaching of the dithionite-reduced HbRC shows that a small population of A_0^{-} is reoxidized in the 6-ns timescale of the measurement. Global analysis gives a lifetime of 14.6 ns for this decay, which is very close to the ~17-ns lifetime corresponding to $P800^{+}A_0^{-}$ charge recombination (*51, 52*).

Table 2. Broad-band pump-probe fitting parameters and statistics

Ascorbate + PMS		Dithionite	
τ	Amplitude	τ	Amplitude
2.9 ± 0.03 ps	1.2	**4.0** ± 0.04 ps	1.3
25.6 ± 0.1 ps	1.4	**33.8** ± 0.1 ps	1.6
725 ± 9.2 ps	-1	**14.6** ± 0.1 ns	-1.2
10.0 ± 2 ns	0.2	-	-
χ^2 = 90.3		χ^2 = 84.6	
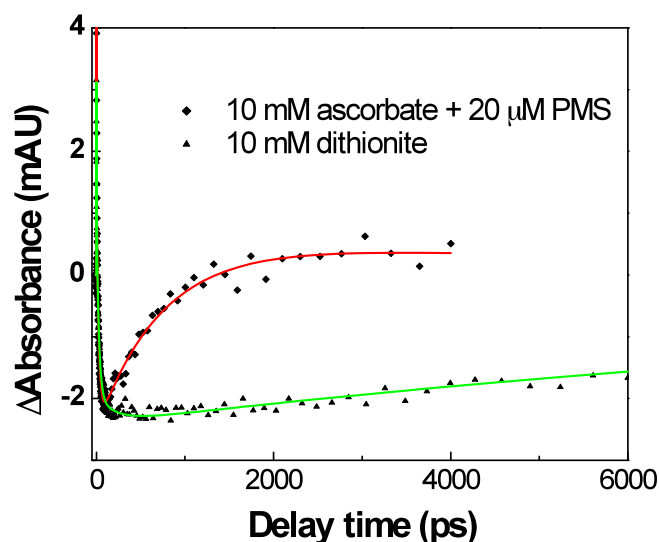
Figure 11. Transient absorption kinetics at 675 nm for HbRC reduced with 10 mM ascorbate and 20 μM PMS (♦) 10 mM dithionite (▲). The data was fit using global analysis with a sum of 4 exponentials for the ascorbate reduced HbRC and 3 exponentials for the dithionite-reduced HbRC. Samples were excited at 575 nm at a frequency of 1 kHz.

Previous reports have attributed the block in electron transfer caused by dithionite treatment at high pH to double reduction of the quinone (*53*). The nature of the cofactor reduced by dithionite cannot be determined using pump-probe spectroscopy, so EPR was used to look for any paramagnetic species generated in the process.

Treatment of the HbRC with 30 mM dithionite in the dark for 30 minutes prior to freezing generates a broad resonance in the 1200-2000 G range detectable by X-band CW-EPR at 3.5 K. This is similar to the signal previously reported to be F_X^- in a S=3/2 state (*20*). The details of this signal will be discussed below along with the signals generated by photoaccumulation methods.

Single-photon counting on dithionite-reduced HbRC

Previous reports have shown that heliobacterial membrane samples in which electron transfer is blocked past A_0 show a long-lived fluorescence component (*52*). This component, with a lifetime of 17 ns, corresponds to charge recombination of the $P800^+A_0^-$ state. This charge recombination can generate one of two excited states in competing

pathways (or regenerate the ground state via dissipation of heat). First, the P800 triplet state (P800^T) can be generated, resulting in relaxation to the ground state via thermal or chemical quenching (*54*). The second pathway regenerates the singlet-excited state of P800 (P800*). This state relaxes back to the ground state via emission of a photon, or fluorescence. This fluorescence is delayed relative to the fluorescence emission from the antenna. Therefore, I expect to observe a long-lived fluorescence component in the HbRC treated with dithionite at pH 10.

Figure 12 shows that reduction of the HbRC with dithionite at pH 10 causes little change in the fluorescence decay at 810 nm emission. The emission at 810 nm from the untreated HbRC decays with a lifetime of 10-20 ps as shown by Table 3 corresponding to the trapping time of the RC. When dithionite is added to this sample, a minor component arises with a lifetime of 2 ns. This component is likely due to uncoupled pigments, as previously reported (*23*). No component with a lifetime of ~20 ns is observed in these samples. However, the transient absorption measurements above show that electron
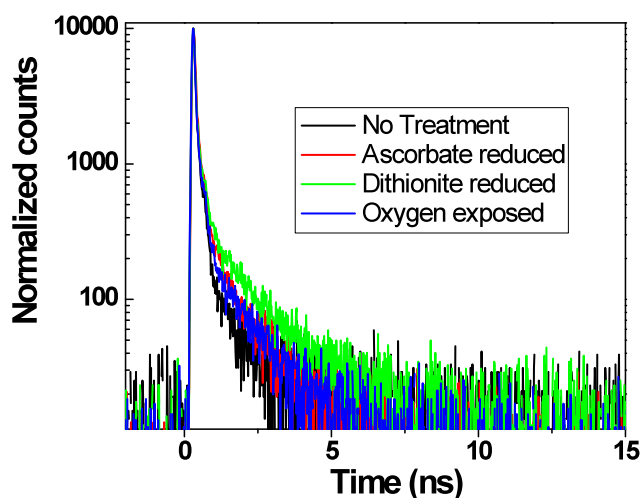
Figure 12. Time-correlated single-photon counting of 810 nm emission using 575 nm excitation on HbRC samples subjected to various chemical treatments. Ascorbate reduced samples were treated with 10 mM ascorbate while dithionite-reduced samples were treated with 10 mM dithionite for 30 minutes in the dark. The dithionite sample was exposed to air for 2 minutes prior to recording the "Oxygen exposed" data. The excitation frequency was 10 MHz.

31

Table 3. TC-SPC fitting parameters and statistics

Sample	τ_1	τ_2	χ_2
HbRC no treatment	15.1 ps (99.96%)	2.35 ns (0.04%)	1.2114
HbRC ascorbate	17.9 ps (99.7%)	1.495 ns (0.28%)	1.3518
HbRC dithionite	8.1 ps (99.80%)	2.08 ns (0.20%)	1.2168
HbRC oxygen	10.22 ps (99.89%)	1.01 ns (0.11%)	1.2923

transfer past A_0 is blocked. One possible explanation is that the P800* state may not be formed by charge recombination of the $P800^+A_0^-$ state in the isolated HbRC. If this were the case, the $P800^T$ formation may be much higher in the isolated HbRC than in the membrane-bound HbRC. The triplet yield in membranes of *H. chlorum* was previously reported to be 30% in RCs from the $P800^+A_0^-$ state, but no studies have determined the yield in the isolated HbRC (*54*). Another possible explanation is that the $P800^+A_0^-$ state may not recombine with the same mechanism and/or kinetics in the isolated HbRC. This is unlikely based on the preliminary results from ultrafast transient absorption above; however, this is beyond the scope of the present work.

Photo-reduction of F_X in carbonate-washed membranes

Previous reports using transient EPR have shown that the $P800^+F_X^-$ state is unstable even at liquid helium temperatures (*50*). Therefore, in order to accumulate detectable levels of F_X^- via photo-reduction, $P800^+$ must be chemically reduced to prevent charge recombination. This process requires a fast chemical donor that can out-compete the 15 ms back-reaction from the $P800^+F_X^-$ state. The natural donor, cytochrome c_{553} reduces $P800^+$ on the microsecond to millisecond timescale, but only when it is tethered to the membrane via a lipid tail. However, the PshB polypeptide that houses the F_A/F_B iron-sulfur clusters is also still present in membrane preparations. Because there may be light-induced changes in the levels of reduced F_A/F_B that may interfere or overlap with the

signal of F_X^-, I developed a procedure to remove the F_A/F_B clusters from membranes prior to photo-accumulation.

While the PshB polypeptide is easily removed during isolation of the HbRC from membranes, removal of PshB in the membrane-bound HbRC has proven to be more difficult (*20, 49*). One possibility is that the liposomes that form in membrane preparations shelter the HbRC (and PshB) from the chaotropic agents. Additionally, even when the interaction between PshB and the HbRC is broken, PshB may be trapped within the liposome as a soluble protein that can re-bind to the HbRC when the chaotropic agents are removed.   These issues can be resolved by washing membranes with sodium carbonate at high pH. This procedure is believed to open liposomes, forming flat membrane sheets and stripping peripheral membrane proteins like PshB (*33*). When the sodium carbonate is removed, the liposomes re-form. Because cytochrome c_{553} is bound to the membrane via a lipid tail, it should not be removed during this procedure (*55*).

The sodium carbonate treatment effectively removes PshB, as shown by the loss of the long-lived component in the flash-induced P800 kinetics. Treatment of these
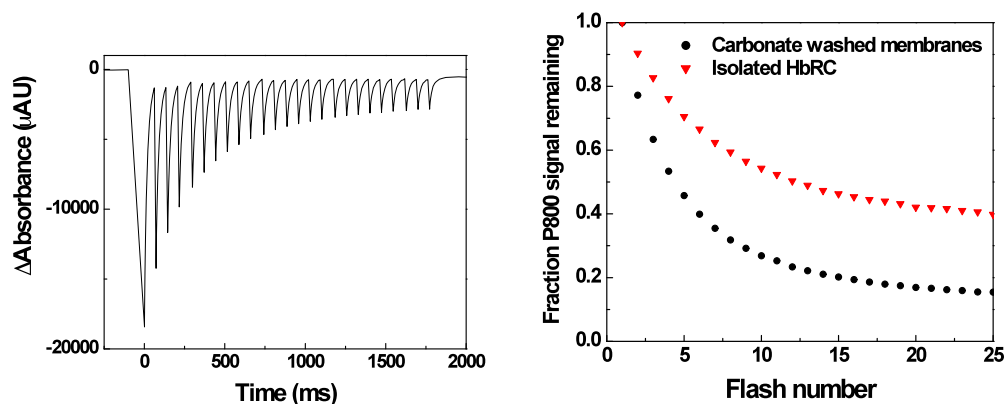
Figure 13. Photoaccumulation of carbonate-washed membranes and HbRC samples in the presence of 10 mM dithionite at pH 6. Left: Representative transient showing the decrease in photobleaching amplitude in carbonate-washed membranes through 25 consecutive laser flashes. Change in sample absorbance at 800 nm was monitored using an 810 nm LED. Right: Fraction of the initial photobleaching amplitude plotted against the number of flashes.

samples with dithionite at pH 6 does not affect the amplitude of the photobleaching signal, indicating that F_X cannot be directly reduced by dithionite at pH 6. If the carbonate-washed membrane samples are subjected to a series of laser flashes in the presence of dithionite at pH 6, the amplitude of the flash-induced bleaching signal decreases as a function of the number of flashes as shown in Figure 13. This indicates that reduced electron acceptors accumulate in these samples, causing P800 recovery on a timescale faster that the 500-microsecond time resolution of the instrument. This result is consistent with successful photo-reduction of F_X in around 85% of HbRCs that will cause recombination of the P800$^+$-A$_0^-$ state with a 17-20 ns lifetime (*51, 52*). Therefore, a light-minus-dark EPR difference spectrum of the carbonate-washed should be dominated by the signal of F_X^-.

There are three distinct signals in the X-band CW-EPR of the as isolated carbonate-washed membranes as shown in Figure 14a. The resonance around g=6 is typical of five-coordinate high-spin iron porphyrins in aqueous solution (*56*). The sharper resonance at g=4.3 is consistent with "nonspecific" iron (*57*). Finally, the resonance in the g=2 region is similar to a 3Fe-4S cluster that is observed in membranes of *Chlorobium tepidum* that results from oxidative damage to a 4Fe-4S cluster (*58*). Upon addition of ascorbate, the resonance around g=2 disappears, indicating the cluster is reduced to an EPR silent state while the other signals are unaffected. When dithionite is added at pH 6, a new signal arises in the g=2 region that is consistent with a 4Fe-4S cluster in the S=1/2 state. The effective g-values of 2.04, 1.94, and 1.89 are similar to those previously reported and assigned to F_X in the HbRC (*50*). However, the reduction potential of dithionite at pH 6 is not low enough to cause direct reduction of F_X shown by the optical measurements discussed above. Additionally, this signal is not observed in the isolated HbRC, therefore this is assigned it to a 2Fe-2S or 4Fe-4S cluster that is not associated with the HbRC. When the dithionite treated sample is illuminated at room
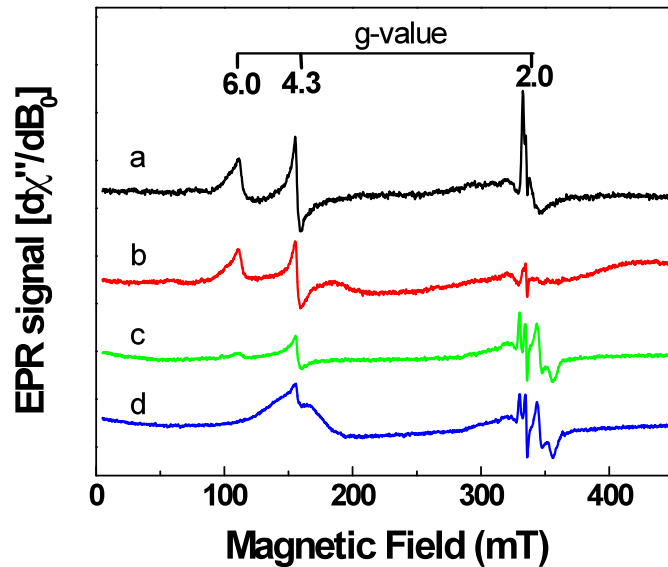
Figure 14. EPR of carbonate-washed membranes. Samples were frozen as-isolated (a), reduced with 10 mM ascorbate (b), or reduced with 10 mM dithionite in the dark (c) or after 30 seconds illumination at room temperature (d). Samples were suspended in 50 mM MES pH 6 containing 20 mM $MgSO_4$. All spectra were recorded at 4.8 K at 1 mW microwave power, 9.43 GHz microwave frequency, 1 mT modulation amplitude, and 100 kHz modulation frequency.

temperature prior to freezing, a broad resonance between 120-200 mT is generated.

This is similar to the signal previously reported to be F_X in the S=3/2 state (*20*). Because

the F_A/F_B clusters have been removed by the washing procedure, the light-minus-dark

difference spectrum should be largely dominated by the signal that can be attributed to

F_X^-. The resulting signal will be further discussed below.

Photo-reduction of F_X in isolated HbRC

The multiple-flash pump-probe method described above was utilized to assess

conditions in which F_X^- could be trapped in the isolated HbRC. Figure 13 shows that in

the presence of dithionite at pH 6, the P800 bleaching signal decreases as a function of

the flash number. This suggests that F_X^- can be trapped in the isolated HbRC under

similar conditions as those used for the carbonate-washed membranes. Though the

efficiency is not as high as in the carbonate-washed membranes, this data suggests that

a P800-F_X^- state can be accumulated in around 50% of RCs. The difference in photo-

reduction efficiency is likely due to the lack of cytochrome c_{553} in the isolated HbRC.

While dithionite can reduce $P800^+$, it is much less efficient than the natural donor.

EPR of F_X

Despite the very different conditions amongst the three samples shown in Figure 15, the spectra are remarkably similar. They are characterized by a broad peak centered at g_{eff}=4.3 with a zero-crossing at g_{eff}=3.7. All three spectra show a sharp resonance near g_{eff}=2 that is most likely unrelated to the F_X signal due to its very narrow linewidth. Additionally, it appears that there is a broad trough centered at g_{eff}=2.0 that is not fully resolved due to the presence of the sharp resonances. The broad features attributed to F_X^- resemble an axial spectrum with $g\perp$=3.7 and g_{II}=2.0. This is consistent with the expected g_{eff}-values of $g\perp\approx4$ and $g_{II}\approx2$ for transitions between the m_s=$\pm$1/2 Kramers
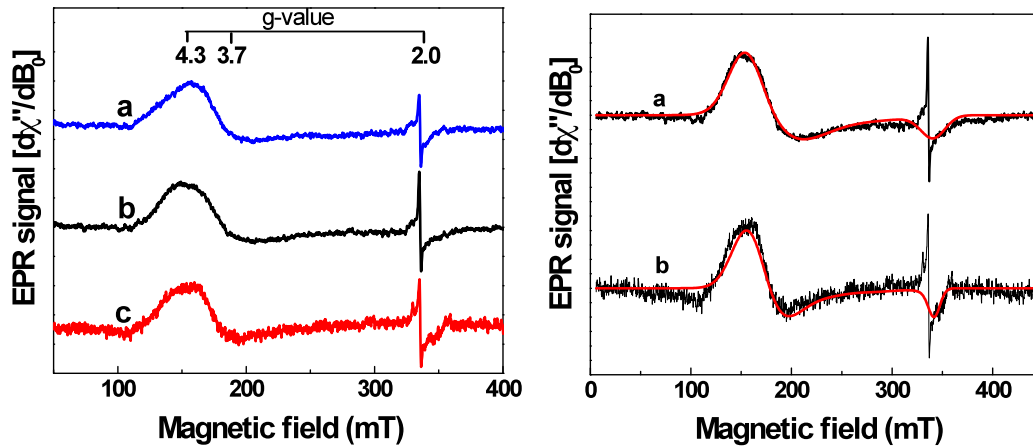
Figure 15. Left: Difference spectra attributed to F_X in HbRC (a and b) and carbonate-washed membrane (c) samples. a. The dithionite-reduced HbRC at pH 6 was subtracted from the dithionite-reduced HbRC at pH 10. b. Light-minus-dark difference spectrum of the dithionite-reduced HbRC at pH 6. c. Light-minus-dark difference spectrum of the dithionite-reduced carbonate-washed membranes. Light treated samples were illuminated for 30 seconds at room temperature prior to freezing. All measurements were performed at 3.5 K at 0.25 mW microwave power, 9.43 GHz microwave frequency, 1 mT modulation amplitude, and 100 kHz modulation frequency. Right: Fitting of the light-minus-dark difference spectra in the isolated HbRC (a) and carbonate-washed membranes (b). Parameters for the fitting of the EPR spectra are shown below in Table 4.

doublet of a S=3/2 system (*59*).   The S=3/2 ground state of F_X^- shown here is consistent with previous reports on F_X in the HbRC (*20*).

The light-minus-dark difference spectra for the isolated HbRC and carbonate-washed membranes were fit to a Hamiltonian with S=3/2 as shown in Figure 13. While the zero-field splitting parameters from the two fits are consistent as shown in Table 4, the g-tensors are significantly different. With an E/D value of 0.02, the zero-field splitting interaction indicates low rhombic distortion of the electronic environment. Additionally, the large positive D value ($>10^5$ MHz) indicates that only the transitions between the $m_s=\pm1/2$ doublet will be observed. This is consistent with the analysis above. The principle g-values and their corresponding linewidths showed significant variation between samples (note that the values in Table 4 are actual rather than effective g-values discussed above). While it is possible that these inconsistencies reflect actual differences in the F_X cluster in the two different environments, they more likely arise due to the broad nature and low intensity of the signal. The subtractions were unable to remove all contaminating signals, especially around $g_{eff}=2$, which is the region of highest discrepancy between the two simulations. Though both simulations show a rhombic g-tensor, further work is needed to improve this aspect of the simulation.

With a linewidth of nearly 50 mT, the F_X signal is unusually broad. Several factors may cause such a large line broadening. Figure 16A shows that the spin-spin

Table 4. EPR spectra simulation parameters

Parameters	Isolated HbRC	Carbonate-washed membranes
	S=3/2	S=3/2
g_x	2.08	2.05
g_y	1.88	2
g_z	1.98	1.97
ΔB_x (mT)	324	317
ΔB_y (mT)	435	357
ΔB_z (mT)	103	44
D (MHz)	$>10^5$	$>10^5$
E/D	0.02	0.02
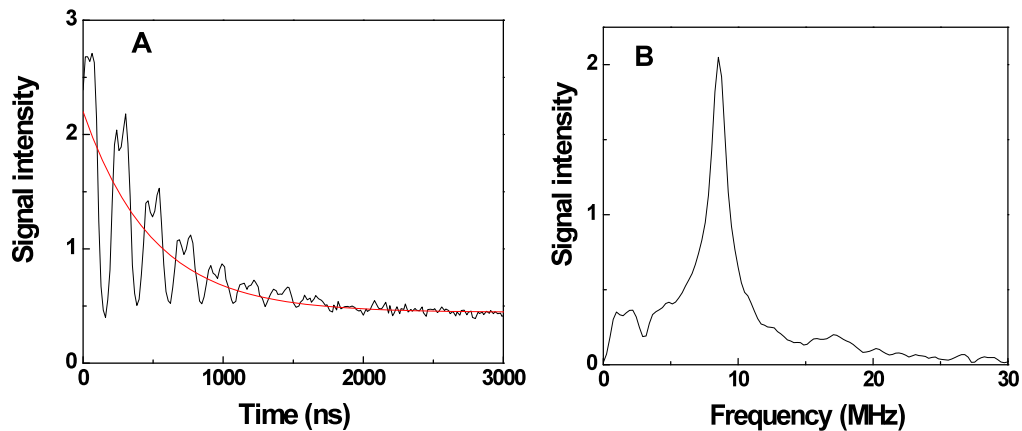
Figure 16. Pulsed X-band EPR measurements on the dithionite -educed HbRC at pH 10. A. T_2 measurement fit to a monoexponential decay with τ = 490 ns. B. Fast-Fourier transform of 3-Pulse ESEEM data taken with a ($\pi/2$-τ-$\pi/2$-t-$\pi/2$-τ-echo) sequence. The length of the $\pi/2$ pulse was 8 ns while the length of τ was 144 ns. Both datasets were collected at a magnetic field position of 209 mT with a microwave frequency of 9.68 GHz.

relaxation (T_2) time of F_X signal is 490 ns at 4 K. Fast spin relaxation times are a major contributing factor to line broadening. Fast spin relaxation times are characteristic of metals, especially metal clusters like F_X. In addition, the T_2 measurement shows strong modulation of the echo decay that is indicative of magnetic interactions between the electron spin of the F_X cluster and nearby magnetic centers. The 3 –pulse ESEEM measurement in Figure 16B show a large peak around 8 MHz, which corresponds to the Larmor frequency of protons at 200 mT applied magnetic field. This suggests that the echo modulation is largely caused by hyperfine interactions with the nuclei of protons. The peaks below 5 MHz likely arise due to nitrogens from the backbone or sidechains of nearby amino acid residues. In addition, there are small, unidentified peaks around 12 and 18 MHz that may come from hyperfine or dipolar interactions. The hyperfine interactions detected by pulsed EPR are not resolved in the CW-EPR spectra and are another major source of line broadening.

Electrochemical properties by thin film voltammetry

In order to study the electrochemical properties of redox cofactors in proteins, the redox state of the cofactor must be monitored as a function of the potential (*60*). The potential of the solution can be varied directly using electrodes or through chemical titrations using oxidants or reductants. The redox state of cofactors can be monitored using a variety of methods such as spectroscopic markers or current flow to and from the solution. Thin film voltammetry is a popular method for studying the electrochemical properties of membrane proteins, especially photosynthetic RCs (*61-63*). In thin film voltammetry, a modifier such as dimyristoylphosphatidylcholine (DMPC) is mixed with the protein of interest at an electrode surface. The modifier should form a monolayer or bilayer on the electrode surface into which the protein of interest can be embedded (*64*). By varying the potential applied to the electrode surface and monitoring current flow, the
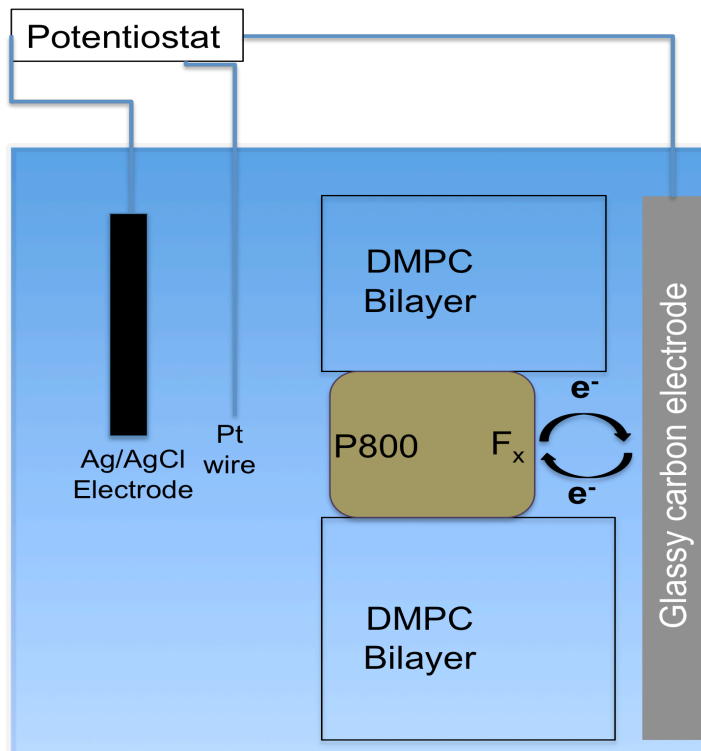
Figure 17. Schematic representation of the set-up for thin-film voltammetry measurements with the HbRC.

midpoint potential of the cofactor can be approximated. As the applied potential nears

the midpoint potential of the cofactor, electrons will flow to (or from) the electrode and

cause a peak in current. Here, a DMPC modifier is used on a glassy carbon (GC)

electrode to study the low-potential acceptors of the isolated HbRC. A representation of

the thin-film voltammetry set-up is shown in Figure 17.

The cyclic voltammogram (CV) of the HbRC on the DMPC modified GC electrode

in Figure 18A shows peaks in both the oxidative and reductive scan direction centered

around -370 mV vs. NHE. Similar results were attained using the more sensitive

technique of differential pulse voltammetry seen in Figure 18B. The average $E_{1/2}$ of this

signal obtained in six independent measurements is -372 ± 17 mV.   This signal is not

present in the DMPC modified GC electrode without the HbRC, so it can be attributed to

a redox center of the HbRC. The presence of peaks in both scan directions is consistent

with the chemical reversibility of reduction of F_X after exposure to oxygen shown above.

Additionally, the separation of the peaks in the CV is less than 59 mV, which is

characteristic for adsorbed species. This indicates that the signal comes from the HbRC

that is bound in close proximity to the electrode.
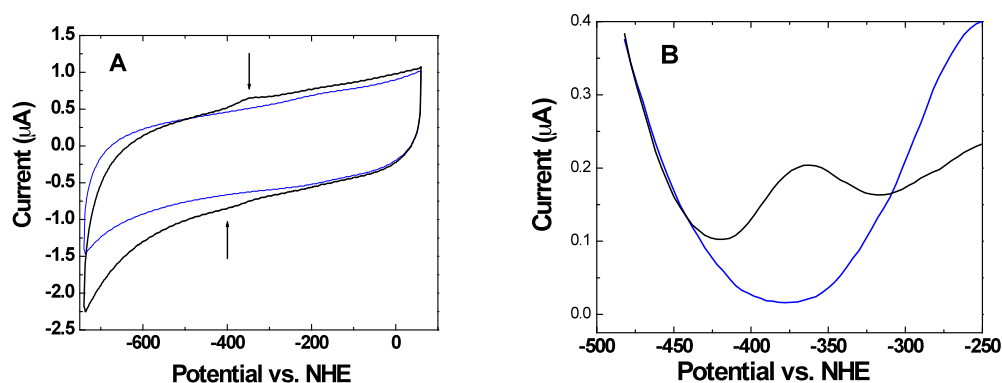
Figure 18. Cyclic (A) and differential pulse (B) voltammograms for the HbRC/DMPC monolayer (black lines) and DMPC coated (blue lines) glassy carbon electrodes. The CV data was collected at a scan rate of 150 mV/s. The DPV data was taken a sample width of 17 ms, pulse amplitude of 25 mV, pulse width of 50 mV, and pulse period of 200 ms. All measurements were performed in 50 mM Tris pH 8 working solution.

The -372 mV value observed here is close to the value of -414 mV previously observed in a reductive titration of the HbRC isolated from *H. gestii* (*53*). In this study, the amplitude of P800 photobleaching on the microsecond timescale was monitored as a function of solution potential, using additions of dithionite in the presence of mediators to change the potential. Because the data fit to a Nernst equation with n=2, it was attributed to double reduction of MQ. However, double reduction of MQ should not block electron transfer to F_X (*28*). The results from EPR and ultrafast absorption suggest that the blockage of electron transfer is a result of the direct reduction of F_X by dithionite. Therefore, the species with a potential of -414 mV identified in previous studies was most likely F_X. The two-electron fit of the data may have been an artifact due to complications caused by the presence of mediators. This will be discussed further in the following section. The species with a potential of -372 mV observed here is tentatively assigned to F_X. A spectroelectrochemical titration should be used as an independent method of confirming this value. However, a method must be designed that avoids the need for mediators.

pH dependence of F_X reduction by dithionite

As described above, the P800 photobleaching signal on the millisecond timescale correlates with the redox state of F_X. This provides a spectroscopic marker that can be used to follow the redox state of F_X as a function of potential. The midpoint potential can be determined by varying the ambient reduction potential of the solution and monitoring the redox state of F_X using pump-probe spectroscopy (*60*). The traditional approach to varying the potential of the solution has been to add small amounts of reductant, such as dithionite, in the presence of redox mediators. The mediators help impose a more stable equilibrium ambient potential and enhance the rate of electron transfer reactions (*60*). However, mediators will interact with all redox active species in solution. This has caused problems with previous titrations involving the HbRC because many of the common mediators used are very effective electron donors to P800$^+$ (*53*).

Mediators like neutral red can reduce P800$^+$ on the sub-millisecond timescale, which will cause a loss of P800 photobleaching signal that is not due to reduction of F_X. An alternative approach that does not require mediators can utilize the pH sensitivity of the reduction potential of dithionite. The mechanism of reduction by dithionite involves the hydroxide ion as a reactant, therefore at higher pH, dithionite has a lower potential (*65*). By varying the pH of the solution from 6 to 10, the midpoint potential of dithionite varies from -176 mV to -648 mV, respectively (*66*). Therefore, the potential of a solution can be varied by changing the pH in the presence of a large excess of dithionite. The large excess of dithionite will enhance the rate of electron transfer and help maintain a stable solution potential, thereby avoiding the need of mediators. If the P800 photobleaching amplitude reaches an equilibrium in the presence of excess dithionite that varies as a function of the pH, this method should allow spectroelectrochemical measurements on F_X.

Figure 19 shows that as pH of the solution changes in the presence of excess dithionite, the P800 photobleaching signal on the millisecond timescale decreases. This is attributed to reduction of F_X that blocks electron transfer and causes charge

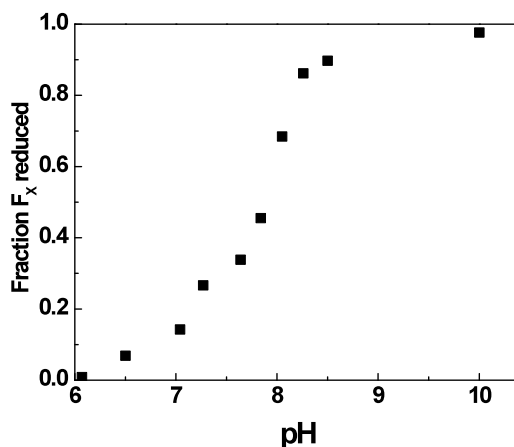**Figure 19.** The pH dependency of F_X reduction by dithionite. The P800 photobleaching signal was measured before and after a 1 hour treatment of 10 mM dithionite at the corresponding pH. The fraction of F_X reduced was defined as the loss in the P800 photobleaching signal following dithionite treatment relative to the initial signal prior to treatment. Each point represents the average of at least 3 measurements.

42

recombination of the $P800^+A_0^-$ state on the nanosecond timescale as shown by the ultrafast absorption and EPR results above. Because the amplitude of the P800 photobleaching in these samples was stable for over 3 hours following dithionite treatment, the redox state of F_X reaches an equilibrium that is dependent on pH. This is most likely due to differences in the ambient solution potential as a result of the pH dependence of the reduction potential of dithionite (*65*). The potentials of the dithionite solutions at each pH were measured in the presence of mediators and the data was fit to the Nernst equation with E_m=-502 mV and n=0.99. Further work will be required to confirm this value.

Discussion

The direct reduction of F_X in the HbRC by dithionite at pH 10 suggests that it has a higher midpoint potential than its counterpart in PSI. The midpoint potential of F_X in PSI is reported to be between -670 and -700 mV while the midpoint potential of F_X in the HbRC has not previously been reported (*67, 68*). Using thin film voltammetry, a redox active species associated with the HbRC was identified with a potential of -372 mV. The preliminary spectroelectrochemical measurements indicate the midpoint potential of F_X in the HbRC in solution is -502 mV. These two values differ by over 100 mV, however, a large disparity is typical between values from thin-film voltammetry and electrochemical titrations (*64*). While both values are significantly higher than the midpoint potential value reported for F_X of PSI, they are consistent with values from other low potential 4Fe-4S clusters such as those of Complex I and bacterial ferredoxins (*69, 70*). With a much higher reduction potential, the reduced state of F_X would be more stable in the HbRC than in PSI. This is consistent with the >10 fold greater lifetime of the $P800^+ F_X^-$ state of the HbRC compared with the $P700^+ F_X^-$ in PSI (*20, 21, 71*).

The large disparity in the potential of F_X in the HbRC and PSI is surprising given that the F_X binding site is the area of highest conservation between the peptides that form the core dimer in these complexes (*18*). A higher potential was predicted for F_X in the

43

HbRC based on a net positive charge in the binding domain, however this would not account for such a large effect (*18*). It is also important to note that the sequence conservation does not necessarily correlate with structural conservation between the dimers at this site. Small differences in the arrangement of the peptides may lead to small differences in the geometry of the cluster, which can correlate to large differences in the potential of the cluster (*72*). Without a crystal structure of the isolated HbRC, such differences are impossible to predict. However, there are major structural differences that can be predicted based on genetic information alone. The isolated HbRC is comprised only of a homodimer of PshA, while PSI contains a total of 12 subunits (*3, 18*). Subunits like PsaC in PSI bury F_X deep within the complex while the F_X cluster in the HbRC must be close enough to the surface of the complex to directly reduce soluble acceptors (*24, 73*). This would give F_X a much higher solvent accessibility in the HbRC, which is a major contributing factor that determines the reduction potential of cofactors in proteins (*74-76*).

Another major difference between the properties of F_X in PSI and the HbRC is the spin state. The ground-state of F_X in PSI is S=1/2 while the results above show that the ground-state of F_X in the HbRC is S=3/2, as was previously reported (*20, 77*). The cause of this difference is unknown, but it hints at structural differences in the protein environment surrounding the cluster. As suggested above, there may be small geometrical differences between the two clusters that may cause a higher potential in the HbRC as well as a different ground spin state. Further investigations using pulsed EPR techniques such as ENDOR and HYSCORE may provide insight on the differences in the interaction of the electron spin of the clusters with the surrounding environment. However, without a crystal structure or the ability to make point mutations to the HbRC, such data would be difficult to interpret.

The simulations of the CW-EPR spectra suggest a low degree of rhombic distortion surrounding the F_X cluster. This lowered anisotropy may be a reflection of the perfect C_2 symmetry that the homodimeric HbRC should exhibit. The rhombic nature of

the g-tensor may indicate anisotropy in the spin distribution on the cluster. However,

further investigations are needed using EPR to improve the interpretation of the F_X^-

signal. The axial zero-field splitting parameter (D) could be determined by measuring at

higher field using Q-band where other transitions involving the $m_s=\pm3/2$ may be observed.

CHAPTER 6. DOUBLE REDUCTION OF MQ BY THE HBRC

Background

One of the major uncertainties surrounding the HbRC (and the Type-I RCs of other anoxygenic bacteria) is the function of the quinones. While quinones are found in the isolated HbRC, they do not seem to be obligate intermediates in electron transfer like the quinones of PSI or Type-II RCs (*26-28*). It has been proposed that the quinones in the HbRC may serve as an alternative electron pathway that is activated when the standard electron acceptor pool is reduced (*78*). When electron transfer from the HbRC is slowed due to accumulation of reduced electron acceptors, electrons will become trapped at the three iron-sulfur clusters of the RC. Eventually, F_X could accumulate in the reduced state and block electron transfer past A_0. In the HbRC with reduced F_X, further excitation leads to a $P800^+A_0^-MQ\ F_X^-$ state that can relax through two pathways. The first pathway would involve charge recombination between $P800^+$ and A_0^-. This can form the triplet state of P800 that may be detrimental to the organism. This has been observed through EPR and ultrafast spectroscopy (*51, 79*). Alternatively, if the quinone can serve as a two-electron acceptor, the $P800^+A_0^-MQ\ F_X^-$ state can relax through double reduction of the quinone to a $P800^+A_0\ MQH_2\ F_X$ state. This pathway would have two major benefits for the organism. First, it would minimize triplet formation in the HbRC. Next, the double reduced quinone could leave the binding pocket and be re-oxidized by the cytochrome b_6c complex. This would contribute to the formation of a proton gradient that can be harvested to make ATP, allowing utilization of energy that would otherwise be lost.

Traditional studies on the function of the quinone in the HbRC have focused on observing a semiquinone state through EPR or ultrafast spectroscopy (*23, 54*). Such studies have been unable to detect a semiquinone radical. An X-band EPR difference spectrum of illuminated the HbRC in the presence of dithionite was originally attributed to a semiquinone radical, but it was later found that this signal most likely came from SO_2^- radicals generated by illumination (*23, 80*). However, if the quinone is double reduced to the quinol state, a semiquinone state may never be observed. The presence of two one-

electron donors in close proximity to the quinone would likely make the lifetime of the semiquinone state too short to detect. Therefore, alternative methods must be used to detect reduction of the quinone to the quinol state. Here, the RP-HPLC method that was developed using *menD1* PSI is used to separate and detect any MQH$_2$ generated in the HbRC after various light and chemical treatments (*45*).

Detection of MQH$_2$

The HPLC method used must be able to separate both MQ and MQH$_2$ from the other pigments and cofactors present in the acetone extracts of the HbRC. Anaerobically isolated membranes can be used as standards as they contain all of the pigments present in the isolated HbRC, as well as MQ and MQH$_2$ in approximately equal abundance (*23*). Separation can be achieved by subjecting the extracts to the same RP-HPLC protocol that was used during studies on PSI. Figure 20A shows a representative trace separating the primary species of interest. The MQ8, MQ9, and MQH$_2$(9) peaks can be integrated to allow independent quantification. While MQH$_2$(8) is not resolved with this method, it can be assumed that the ratio of MQ:MQH$_2$ for MQ8 and MQ9 are approximately equal.

Photoaccumulation of the isolated HbRC

Earlier I showed via RP-HPLC that *menD1* PSI doubly reduces PQ in the presence of ascorbate and PMS after 64,000 saturating laser flashes. Ascorbate serves as a mild reductant while PMS serves as a fast electron donor that catalyzes the re-reduction of the oxidized special pair. When a similar light and chemical treatment is applied to the HbRC, no MQH$_2$ is detected. This method is capable of detecting conversion of <2% of the MQ9 to MQH$_2$, therefore the quinone reducing activity of the HbRC under these conditions is very low. Additionally, there is significant damage to the HbRC as shown by conversion of Bchl *g* to Chl *a* as well as loss in P800 photobleaching signal (not shown). One possible problem is that PMS is not a fast enough reductant to

out-compete the 14 ms back-reaction of the P800$^+$ F$_X^-$ state. The results from EPR and

pump-probe spectroscopy above show dithionite can out-compete this back-reaction,

leading to a rapid accumulation of reaction centers a P800-F$_X^-$ state. This will enable use

of more mild light treatments that will minimize photodamage to the HbRC.

Treatment of the HbRC with dithionite may cause artifactual reduction of MQ that

is not due to the light treatment. To avoid "dark reduction" of extracted quinones,

dithionite was removed by passing HbRC samples over a 50-kDa cutoff membrane.

Extracts of HbRC samples treated with dithionite at pH 6 in the dark that were prepared

in this manner show no detectable levels of MQH$_2$. However, around 50% of the

quinones in HbRC samples are reduced following treatment with dithionite at pH 10 in the

dark. The fraction reduced varies depending on the length of time between the removal

of dithionite from the samples and the extraction. This suggests that MQH$_2$ generated

during dithionite treatment is re-oxidized by the lengthy procedure (~30 minutes) of

dithionite removal. Therefore, the redox state of the quinones in the HbRC samples

treated with dithionite cannot be measured accurately.

Photoaccumulation of HbRC in membranes

In heliobacterial membrane samples, cytochrome c_{553} serves as an electron

donor to the HbRC, reducing P800$^+$ on the millisecond timescale. Cytochrome c_{553} can

be reduced by ascorbate, making dithionite treatment for membrane samples

unnecessary. This will simplify and shorten the extraction protocol and minimize the risk

of dark reduction of quinones. However, I showed above that around half of the quinones

in anaerobically isolated membrane samples are reduced. Samples with quinones in the

fully oxidized state are preferential for these studies. This can be achieved by isolating

the heliobacterial membranes in aerobic environments under vary low light to minimize

damage to the HbRC. The quinones of samples isolated in this manner are fully

oxidized, suggesting that MQH$_2$ can be oxidized by oxygen either directly or with the aide

of a membrane-bound complex. Because MQH$_2$ in membranes may be re-oxidized by
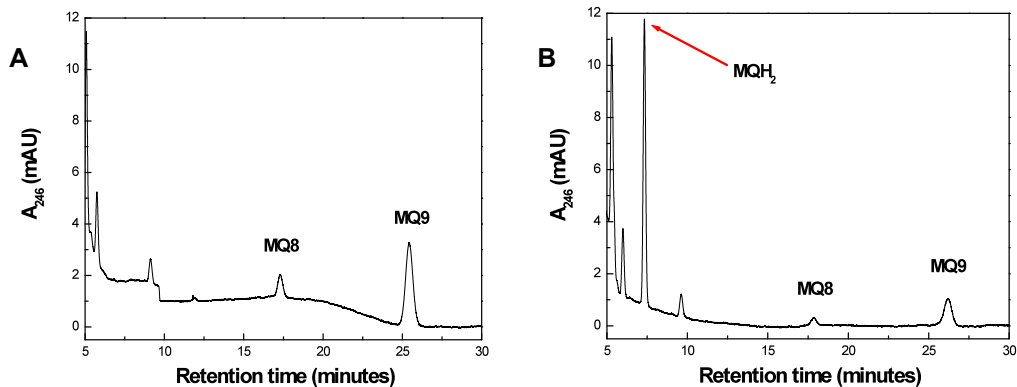
Figure 20. HPLC chromatograms showing separation of MQH_2 and MQ using the absorbance of the eluent monitored at 246 nm. A. Carbonate-washed membranes were treated with 20 mM ascorbate at pH 6 in the dark. B. Carbonate-washed membranes were treated with 20 mM ascoorbate at pH 6 and subjected to 5,000 laser flashes prior to extraction. The 100 μL samples were rapidly extracted with 500 μL acetone following light (or dark) treatment.

complexes such as the cytochrome b_6c complex, it is important to extract the quinones as rapidly as possible following the light treatment. Finally, carbonate-washed membranes were used rather than the native membranes to increase the photoaccumulation efficiency by removing PshB. In the presence of PshB (and F_A/F_B) double reduction of the quinone is a four-photon, four-electron process as compared the two-photon, two electron-process in carbonate-washed membranes. This is because reduction of the quinone presumably requires stable reduction of F_X, which will not occur if F_A/F_B are oxidized.

As shown in Figure 20A, the quinones in the aerobically isolated carbonate-washed membrane samples treated with ascorbate in the dark are fully oxidized. Ascorbate is only a mild reductant so it is not surprising that it cannot reduce MQH_2 in the dark. Figure 20B shows that MQH_2 can be generated in carbonate-washed membranes treated with ascorbate following 5,000 laser flashes. Comparison of the integrated peak areas suggests that 60% of the quinones in the extract are in the MQH_2 form. However, the ratio of quinones (MQ + MQH_2) to Bchl *g* suggests that there are only ~2 quinones per HbRC in the sample while the expected ratio is 4-5 quinone per HbRC in membranes

(for both light and dark treated samples). The low quinone content is due to the high water content in the acetone extracts. This will limit the solubility of the very hydrophobic cofactors such as the quinone and carotenoid and lead to lower extraction efficiency compared to less hydrophobic cofactors like Bchl *g*. The similar quinone content of the light and dark treated samples suggests that MQ and MQH_2 have similar extraction efficiencies. Therefore, the redox state of the quinones in the extract should reflect the redox state of the quinones in the membrane sample. However, the quinone extraction procedure must be redesigned to enable complete extraction of quinones and allow complete quantification.

Discussion

The light-dependent reduction of MQ to MQH_2 in heliobacterial membrane samples shown here suggests that the HbRC is capable of doubly reducing quinones. This is the first direct evidence for double reduction of quinones in the HbRC. Further studies will be needed to evaluate the physiological relevance of this activity. Unlike PSI, the quinone is not an obligate intermediate in electron transfer for the HbRC (*28*). Therefore, double reduction of the quinone in the HbRC should have no deleterious effects. In fact, this activity may potentially be advantageous for the organism if the quinol can leave the binding site. It would provide the HbRC an alterative electron acceptor when the pool of soluble acceptors becomes reduced. Past studies in cells of *H. modesticaldum* have shown that electron transport from the HbRC to soluble electron acceptors can easily be blocked (*81*). In this case, electrons are trapped on the intermediate acceptors of the HbRC like A_0 and F_X, inactivating the RCs. The quinones present in the HbRC may reoxidize these intermediate electron acceptors and reactivate these RCs. Additionally, the reduced quinones may be oxidized by the cytochrome b_6c complex, contributing to the formation of a proton gradient that allows formation of ATP.

Future studies should test the efficiency of quinone reduction by the HbRC by determining the fraction of MQ reduced to MQH_2 as a function of the number of charge-

separation events (saturating laser flashes). This could help determine whether this function is likely to occur in a natural system or only under extreme lighting conditions that the organism is unlikely to experience. Additionally, the activity should be studied in the presences of various compounds that should inhibit the process. Methyl and benzyl viologen can be used to prevent stable reduction of F_X, which should decrease the quinone-reducing efficiency of the HbRC. Also, inhibitors of the Q_B-binding site of Type II RCs like terbutryn may decrease the efficiency of photoreduction of the quinone by the HbRC by blocking the MQ binding sites. If this were the case, it would suggest MQH_2 and/or MQ could diffuse from the binding site of the HbRC and allow cyclic electron transfer between the HbRC and the cytochrome b_6c complex. This would greatly strengthen the case that quinone double-reduction is a physiologically relevant function of the HbRC *in vivo*.

CHAPTER 7. DISCUSSION

Antenna size

The antenna size of the HbRC is rather small at 22 Bchl g per reaction center, as shown in Chapter 4. PSI on the other hand binds almost 100 chlorophylls per reaction center (*3*). One potential reason for this large disparity could be the different environments in which the organisms that utilize these complexes are found. Cyanobacteria, which utilize PSI, are generally found in aquatic systems where iron is often a limiting nutrient (*82-84*). A functioning complex requires at least 12 irons per monomeric PSI (*3*). Therefore, it is advantageous for cyanobacteria to utilize large antenna (as well as external antenna complexes) in order to minimize the number of PSI complexes (and iron) required to utilize the available light. On the other hand, heliobacteria are generally found in soil systems where iron is comparably more available (*85*). Furthermore, the functional HbRC may only require 4 irons, though this has never been demonstrated *in vivo* (*24*). Therefore, iron limitation may not have been an important driving factor in the evolution of the HbRC. In order to harvest more light energy, heliobacteria would likely just synthesize more RCs. Additionally, the main pigment of the HbRC, Bchl g, is much more labile than chlorophyll a (*15, 86*). Therefore a large antenna size may be disadvantageous in the HbRC due to the potential damage to the antenna pigments. If damage to antenna pigments were a driving factor in the evolution of the HbRC, it would be advantageous to maintain a low ratio of pigments per reaction center.

Electrochemical properties of F_X

The results of Chapter 5 suggest the midpoint potential of F_X in the HbRC is much higher than the midpoint potential of F_X in PSI (*67, 68*). The potential for F_X in the HbRC shown here is consistent with the values of other low potential 4Fe-4S clusters. Therefore, it is likely that the last common ancestor between PSI and the HbRC had a 4Fe-4S cluster with a potential similar to the value for F_X in the HbRC. The low potential

of F_X in PSI may have arisen directly or indirectly as a result of selective evolution. In other words, a lower potential for the cluster may have been evolutionarily advantageous or resulted indirectly as a consequence of selection for another property.

The low potential of F_X in ancestral forms of PSI may have been advantageous to destabilize the $P700^+ F_X^-$ state. The rate of forward electron transfer from F_X to F_A/F_B is still faster than the back-reaction by orders of magnitude. Therefore, back-reaction from F_X should only occur when electron transfer to F_A/F_B is blocked. In this case, charge recombination would be advantageous. Increasing the rate of this back-reaction would minimize the risk of doubly reducing the quinones bound at the A_1 position (discussed further below) that inactivates PSI (*38, 39, 45*). Double reduction of the quinone should not inactivate the RC, so destabilizing the $P800^+ F_X^-$ state would not be advantageous (*28*). In fact, destabilizing the $P800^+ F_X^-$ may have been disadvantageous. The PshB peptide that houses the F_A/F_B clusters in heliobacteria may not form a tight interaction with the HbRC in the way that PsaC (housing F_A/F_B) is tightly bound to PSI (*87*). For the majority of the evolution of heliobacteria (and the HbRC), it is likely that HbRC *in vivo* resembled the isolated HbRC described above, where F_X is the terminal electron acceptor that reduced soluble ferredoxins and other soluble electron carriers. In this case, a long-lived $P800^+ F_X^-$ state would be advantageous to account for the slower, diffusion-limited electron transfer to F_A/F_B (or other acceptors). Indeed, the lifetime of $P800^+ F_X^-$ state is over 10 fold greater than the lifetime of the $P700^+ F_X^-$ state (*20, 21, 71*).

Conversely, the lower potential of F_X in PSI may not have been directly selected for as proposed above. As suggested in Chapter 5, the lower potential of F_X in PSI may be due to decreased solvent accessibility relative to F_X in the HbRC. The lower solvent accessibility in PSI is due to the presence of 10 additional subunits in cyanobacterial PSI compared to the isolated HbRC (*3, 48*). The additional subunits in PSI most likely conferred some unrelated selective advantage but may have lowered the potential of F_X as a result. Another possible reason for the large difference in potential may be differences in geometry of the two clusters. Geometrical differences to the clusters may

arise due to, among other things, the heterodimeric nature of PSI compared to the homodimeric nature of the HbRC. The evolutionary advantage of a PSI heterodimer is still unclear, but probably did not directly relate to changing the potential of F_X.

Double reduction of quinones by PSI and the HbRC

All known photosynthetic RCs can be classified as either Type-I or Type-II and likely evolved from a universal common ancestor (*2*). The properties of the last common ancestor of modern photosynthetic RCs have been a subject of debate for 30 years. Namely, did it reduce iron-sulfur clusters as in Type-I RCs, or quinones as in Type-II RCs? Alternatively, some have proposed it may have functioned as both a Type-I and Type-II RC, making it a "Type-1.5" RC (*78*). This Type-1.5 RC would be capable of reducing soluble electron acceptors like a Type-I RC, as well as internally bound quinones like a Type-II RC. Genetic data, which has long been the cornerstone of evolutionary studies, is unable to resolve such detailed questions of function. Therefore, determining the full range of functional capabilities of the modern RCs is important for improving the understanding of the evolution of photosynthesis.

The present work shows that PSI is capable of doubly reducing quinones. However, the quinone double-reduction activity is unlikely to be of any physiological relevance. It requires either strong reducing conditions imposed by dithionite (as shown previously) or recruitment of a foreign quinone (*38, 39, 45*). Above, I showed the first evidence that the HbRC is capable of doubly reducing quinones. As discussed in Chapter 6, this may be a physiologically relevant activity of the HbRC *in vivo*, though further studies will be required to test this hypothesis. The mechanism quinone double-reduction activity of these RCs may provide insight on the early evolution of photosynthetic RCs. All known photosynthetic RCs bind quinones, which many believe suggests that the universal common ancestor to all RCs utilized a quinone as a terminal electron acceptor. While the last common ancestor may have used a quinone as a two-electron acceptor, it is unlikely that it utilized a Type-II mechanism. The Type-II

mechanism described in Chapter 1 relies on functional asymmetry of the two branches of cofactors. However, the last common ancestor was almost certainly homodimeric. It is unlikely that homodimeric peptide environment could develop functional asymmetry between the two branches of cofactors. Therefore, it is important to determine the mechanism of quinone reduction in the functionally symmetric Type-I RCs shown above.

In PSI, a "pseudo" Type-II mechanism is theoretically possible. That is, the double reduction of PQ may be the result of a dismutation reaction between two semiquinones on opposite branches of the PSI complex. This is unlikely because once the PQ on one branch became fully reduced the dismutation reaction would no longer be possible. Therefore, only 50% of quinones could be reduced via this mechanism. The results in Chapter 3 show that ~75% of the quinones are doubly reduced, so an alternative mechanism must be utilized. Another mechanism involves reduction of a semiquinone by the primary acceptor A_0. In the case where F_X is reduced, further charge separation will yield a $P700^+ A_0 PQ^- F_X^-$ state. Next, $P700^+$ would need to be re-reduced before back-reaction from PQ^-. Finally, a second charge separation will generate a $P700^+ A_0^- PQ^- F_X^-$ state where PQ^- can be fully reduced by A_0^-. Though this mechanism could account for the >50% reduction of PQ observed, it is unlikely due to the short lifetime of the $P700^+ PQ^-$ state. The lifetime of $P700^+ PQ^-$ is ~8 μs while PMS re-reduces $P700^+$ with a maximal rate of 2.4 ms (*88, 89*). Therefore, generation of a $P700^+ A_0^- PQ^- F_X^-$ state is improbable. The final mechanism for double reduction of PQ in PSI is analogous to the mechanism for double reduction of quinones in the HbRC proposed in Chapter 6 following accumulation of a $P700 A_0 PQ^- F_X^-$ state. Further excitation would lead to reduced states of A_0 and F_X, which could reduce PQ sequentially, generating a semiquinone intermediate, or simultaneously to fully reduce PQ to PQH_2. Of the three mechanisms discussed here, this is the most likely because it can account for reduction of >50% of PQ to PQH_2 and does not rely on a long-lived semiquinone intermediate state. Because a semiquinone state has never been observed in the HbRC, this is also the most likely mechanism by which the quinone in the HbRC would be doubly reduced.

The mechanism for quinone double reduction in two functionally symmetric Type-I RCs shown here provides insight on how Type-I and Type-II RCs may have diverged from a common ancestor. Due to the common features observed in Type-I and Type-II RCs, all modern RCs most likely diverged from a homodimer that bound two quinones (*78*). It is possible that these quinones served as two electron acceptors similar to the modern Type-II RCs, though it would require a distinct mechanism due to the functional asymmetry of the Type-II mechanism. The modern RCs transfer a single electron per excitation; however, the one-electron reduced state of a quinone is generally unstable. The asymmetry of the Type-II RCs most likely evolved to stabilize the semiquinone to allow for a second charge separation, and second electron to fully reduce the semiquinone. Alternatively, the last common ancestor may have utilized a more stable one-electron acceptor such as an iron-sulfur cluster, mononuclear iron, or heme to store the first electron rather than the quinone itself. Type-I RCs may have branched off when the intermediate acceptor developed the ability to reduce soluble electron acceptors. The Type-II RCs developed the ability to stabilize the semiquinone state, foregoing the need for an intermediate electron carrier. This divergence occurred over 3 billion years ago making it unlikely that the evolutionary development of the modern photosynthetic RCs will ever be understood (*13*).

REFERENCES

1.   Calvin, M., Bassham, J. A., and Benson, A. A. (1950) Chemical transformations of carbon in photosynthesis, *Federation Proceedings 9*, 524-534.

2.   Blankenship, R. E. (1992) Origin and early evolution of photosynthesis, *Photosynth. Res. 33*, 91-111.

3.   Jordan, P., Fromme, P., Witt, H. T., Klukas, O., Saenger, W., and Krauss, N. (2001) Three-dimensional structure of cyanobacterial photosystem I at 2.5 A resolution, *Nature 411*, 909-917.

4.   Schoeder, H.-U., and Lockau, W. (1986) Phylloquinone copurifies with the large subunit of photosystem I., *FEBS Lett. 199*, 23-27.

5.   McDermott, A. E., Yachandra, V. K., Guiles, R. D., Sauer, K., Klein, M. P., Parrett, K. G., and Golbeck, J. H. (1989) EXAFS structural study of FX, the low-potential Fe-S center in photosystem I, *Biochemistry 28*, 8056-8059.

6.   Codgell, R. J., Southall, J., Gardiner, A. T., Law, C. J., Gall, A., Roszak, A. W., and Isaacs, N. W. (2006) How purple photosynthetic bacteria harvest solar energy, *C. R. Chim. 9*, 201-206.

7.   Isaacson, R. A., Lendzian, F., Abresch, E. C., Lubitz, W., and Feher, G. (1995) Electronic structure of Q-A in reaction centers from *Rhodobacter sphaeroides*. I. Electron paramagnetic resonance in single crystals, *Biophys J 69*, 311-322.

8.   Graige, M. S., Feher, G., and Okamura, M. Y. (1998) Conformational gating of the electron transfer reaction QA-.QB --> QAQB-. in bacterial reaction centers of *Rhodobacter sphaeroides* determined by a driving force assay, *Proc Natl Acad Sci U S A 95*, 11679-11684.

9.   Guergova-Kuras, M., Boudreaux, B., Joliot, A., Joliot, P., and Redding, K. (2001) Evidence for two active branches for electron transfer in photosystem I, *Proc Natl Acad Sci U S A 98*, 4437-4442.

10.   Katilius, E., Turanchik, T., Lin, S., Taguchi, A. K. W., and Woodbury, N. W. (1999) B-Side Electron Transfer in a *Rhodobacter sphaeroides* Reaction Center Mutant in Which the B-Side Monomer Bacteriochlorophyll Is Replaced with Bacteriopheophytin, *J. Phys .Chem. B 103*, 7386-7389.

11.   Deisenhofer, J., Epp, O., Miki, K., Huber, R., and Michel, H. (1984) X-ray structure analysis of a membrane protein complex. Electron density map at 3 A resolution and a model of the chromophores of the photosynthetic reaction center from *Rhodopseudomonas viridis*, *J Mol Biol 180*, 385-398.

12.   Morris, E. P., Hankamer, B., Zheleva, D., Friso, G., and Barber, J. (1997) The three-dimensional structure of a photosystem II core complex determined by electron crystallography, *Structure 5*, 837-849.

13.   Hohmann-Marriott, M. F., and Blankenship, R. E. (2011) Evolution of Photosynthesis, In *Annual Review of Plant Biology, Vol 62* (Merchant, S. S., Briggs, W. R., and Ort, D., Eds.), pp 515-548, Annual Reviews, Palo Alto.

14. Gest, H., Favinger, J.L., . (1983) *Heliobacterium chlorum*, an anoxygenic brownish-green photosynthetic bacterium containing a "new" form of bacteriochlorophyll *Arch.Microbiology 136*, 11-16.

15. Brockman Jr., H. a. L. (1983) Bacteriochlorophyll g. A new bacteriochlorophyll pigment from *Heliobacterium chlorum*, *Archives of Microbiology 136*, 17-19.

16. Fuller, R. C., Sprague, S. G., Gest, H., and Blankenship, R. E. (1985) A unique photosynthetic reaction center from *Heliobacterium chlorum*, *FEBS Lett. 182*, 345-349.

17. Sattley, W. M., Madigan, M. T., Swingley, W. D., Cheung, P. C., Clocksin, K. M., Conrad, A. L., Dejesa, L. C., Honchak, B. M., Jung, D. O., Karbach, L. E., Kurdoglu, A., Lahiri, S., Mastrian, S. D., Page, L. E., Taylor, H. L., Wang, Z. T., Raymond, J., Chen, M., Blankenship, R. E., and Touchman, J. W. (2008) The genome of *Heliobacterium modesticaldum*, a phototrophic representative of the Firmicutes containing the simplest photosynthetic apparatus, *J Bacteriol 190*, 4687-4696.

18. Liebl, U., Mockensturmwilson, M., Trost, J. T., Brune, D. C., Blankenship, R. E., and Vermaas, W. (1993) Single core polypeptide in the reaction center of the photosynthetic bacterium *Heliobacterium mobilis* - Structural implications and relations to other photosystems, *Proc. Natl. Acad. Sci. U. S. A. 90*, 7124-7128.

19. Hirozo, O.-O. (2007) Type 1 Reaction Center of Photosynthetic Heliobacteria, *Photochemisty and Photobiology, 83*, 177-186.

20. Heinnickel, M., Agalarov, R., Svensen, N., Krebs, C., and Golbeck, J. H. (2006) Identification of F(X) in the Heliobacterial Reaction Center as a [4Fe-4S] Cluster with an S = (3)/(2) Ground Spin State, *Biochemistry 45*, 6756-6764.

21. Trost, J. T., and Blankenship, R. E. (1989) Isolation of a photoactive photosynthetic reaction center-core antenna complex from *Heliobacillus mobilis*, *Biochemistry 28*, 9898-9904.

22. Vermaas, W. F. J. (1994) Evolution of heliobacteria-Implications for photosynthetic reaction center complexes, *Photosynth. Res. 41*, 285-294.

23. Sarrou, I., Khan, Z., Cowgill, J., Lin, S., Brune, D., Romberger, S., Golbeck, J. H., and Redding, K. E. (2012) Purification of the photosynthetic reaction center from *Heliobacterium modesticaldum*, *Photosynth. Res. 111*, 291-302.

24. Romberger, S. P., and Golbeck, J. H. (2012) The F-X iron-sulfur cluster serves as the terminal bound electron acceptor in heliobacterial reaction centers, *Photosynth. Res. 111*, 285-290.

25. van de Meent, E. J., Kobayashi, M., Erkelens, C., van Veelen, P. A., and Amesz, J. (1991) Identification of 8^1-hydroxychlorophyll *a* as a functional reaction center pigment in heliobacteria, *Biochim Biophys Acta 1058*, 356-362.

26. Lin, S., Chiou, H. C., Kleinherenbrink, F. A., and Blankenship, R. E. (1994) Time-resolved spectroscopy of energy and electron transfer processes in the photosynthetic bacterium *Heliobacillus mobilis*, *Biophys J 66*, 437-445.

27.   Nuijs, A. M., Van Dorssen, R. J., Duysens, L. N. M., and Amesz, J. (1985) Excited states and primary photochemical reactions in the photosynthetic bacterium *Heliobacterium chlorum*, *Proc. Natl. Acad. Sci. U. S. A. 82*, 6965-6968.

28.   Kleinherenbrink, F. A. M., Ikegami, I., Hiraishi, A., Otte, S. C. M., and Amesz, J. (1993) Electron-transfer in menaquinone-depleted membranes of *Heliobacterium chlorum*, *Biochimica Et Biophysica Acta 1142*, 69-73.

29.   Kruk, J., and Karpinski, S. (2006) An HPLC-based method of estimation of the total redox state of plastoquinone in chloroplasts, the size of the photochemically active plastoquinone-pool and its redox state in thylakoids of Arabidopsis, *Biochim. Biophys. Acta-Bioenerg. 1757*, 1669-1675.

30.   Siefermann-Harms, D. (1998) High-performance liquid chromatography of chloroplast pigments. One-step separation of carotene and xanthophyll isomers, chlorophylls and pheophytins, *Journal of chromatography 448*, 411-416.

31.   Suzuki, H., Sugiura, M., and Noguchi, T. (2009) Monitoring Proton Release during Photosynthetic Water Oxidation in Photosystem II by Means of Isotope-Edited Infrared Spectroscopy, *J. Am. Chem. Soc. 131*, 7849-7857.

32.   Hale M, B. R., Fuller RC (1983) Menaquinone is the sole quinone in the facultatively aerobic green photosyntheitic bacterium *Chloroplexus aurantiacus*, *Biochim Biophys Acta 723*, 376-382.

33.   Fujiki, Y., Hubbard, A. L., Fowler, S., and Lazarow, P. B. (1982) Isolation of intracellular membranes by means of sodium carbonate treatment - Application to endoplasmic reticulum, *J. Cell Biol. 93*, 97-102.

34.   Pan, J., Lin, S., Allen, J. P., Williams, J. C., Frank, H. A., and Woodbury, N. W. (2011) Carotenoid Excited-State Properties in Photosynthetic Purple Bacterial Reaction Centers: Effects of the Protein Environment, *J. Phys. Chem. B 115*, 7058-7068.

35.   Stoll, S., and Schweiger, A. (2006) EasySpin, a comprehensive software package for spectral simulation and analysis in EPR, *J. Magn. Reson. 178*, 42-55.

36.   Flores, M., Isaacson, R., Abresch, E., Calvo, R., Lubitz, W., and Feher, G. (2007) Protein-cofactor interactions in bacterial reaction centers from *Rhodobacter sphaeroides R-26: II*. Geometry of the hydrogen bonds to the primary quinone Q(A)(-) by H-1 and H-2 ENDOR spectroscopy, *Biophys. J. 92*, 671-682.

37.   Srinivasan, N., and Golbeck, J. H. (2009) Protein-cofactor interactions in bioenergetic complexes: The role of the A(1A) and A(1B) phylloquinones in Photosystem I, *Biochim. Biophys. Acta-Bioenerg. 1787*, 1057-1088.

38.   Inoue, K., Fujii, T., Yokoyama, E., Matsuura, K., Hiyama, T., and Sakurai, H. (1989) The photoinhibition site of Photosystem-I in isolated chloroplasts under extremely reducinng conditions, *Plant Cell Physiol. 30*, 65-71.

39.   Sétif, P., and Bottin, H. (1989) Identification of electron-transfer reactions involving the acceptor A1 of photosystem I at room temperature, *Biochemistry 28*, 2689-2697.

40.   Iwaki, M., and Itoh, S. (1989) Electron transfer in spinach Photosystem I reaction center containing benzoquinone, naphthoquinone and anthraquinones in place of phylloquinone, *FEBS Lett. 256*, 11-16.

41.   Iwaki, M., and Itoh, S. (1994) Reaction of reconstituted acceptor quinone and dynamic equilibration of electron transfer in the photosystem I reaction center, *Plant Cell Physiol. 35*, 983-993.

42.   Johnson, T. W., Shen, G. Z., Zybailov, B., Kolling, D., Reategui, R., Beauparlant, S., Vassiliev, I. R., Bryant, D. A., Jones, A. D., Golbeck, J. H., and Chitnis, P. R. (2000) Recruitment of a foreign quinone into the A(1) site of photosystem I - I. Genetic and physiological characterization of phylloquinone biosynthetic pathway mutants in *Synechocystis sp PCC 6803, J. Biol. Chem. 275*, 8523-8530.

43.   Semenov, A. Y., Vassiliev, I. R., van Der Est, A., Mamedov, M. D., Zybailov, B., Shen, G., Stehlik, D., Diner, B. A., Chitnis, P. R., and Golbeck, J. H. (2000) Recruitment of a foreign quinone into the A1 site of photosystem I. Altered kinetics of electron transfer in phylloquinone biosynthetic pathway mutants studied by time-resolved optical, EPR, and electrometric techniques, *J Biol Chem 275*, 23429-23438.

44.   Ozawa, S. I., Kosugi, M., Kashino, Y., Sugimura, T., and Takahashi, Y. (2012) 5'-Monohydroxyphylloquinone is the Dominant Naphthoquinone of PSI in the Green Alga *Chlamydomonas reinhardtii, Plant Cell Physiol. 53*, 237-243.

45.   McConnell, M. D., Cowgill, J. B., Baker, P. L., Rappaport, F., and Redding, K. E. (2011) Double Reduction of Plastoquinone to Plastoquinol in Photosystem 1, *Biochemistry 50*, 11034-11046.

46.   Kaupp, M. (2002) The function of photosystem I. Quantum chemical insight into the role of tryptophan-quinone interactions, *Biochemistry 41*, 2895-2900.

47.   Kobayashi, M., van de Meent, E. J., Erkelens, C., Amesz, J., Ikegami, I., and Watanabe, T. (1991) Bacteriochlorophyll *g* epimer as a possible reaction center component of heliobacteria, *Biochim Biophys Acta 1057*, 89-96.

48.   Liebl, U., Mockensturm-Wilson, M., Trost, J., Brune, D., Blankenship, R., and Vermaas, W. (1993) Single core polypeptide in the reaction center of the photosynthetic bacterium *Heliobacillus mobilis*: structural implications and relations to other photosystems, *Proc. Natl. Acad. Sci. U. S. A. 90*, 7124-7128.

49.   Kleinherenbrink, F. A. M., Chiou, H.-C., LoBrutto, R., and Blankenship, R. E. (1994) Spectroscopic evidence for the presence of an iron-sulfur center similar to FX of photosystem I in *Heliobacillus mobilis*, *Photosynth. Res. 41*, 115-123.

50.   Miyamoto, R., Iwaki, M., Mino, H., Harada, J., Itoh, S., and Oh-Oka, H. (2006) ESR signal of the iron-sulfur center F(X) and its function in the homodimeric reaction center of *Heliobacterium modesticaldum*, *Biochemistry 45*, 6306-6316.

51.   Kleinherenbrink, F. A. M., Aartsma, T. J., and Amesz, J. (1991) Charge separation and formation of bacteriochlorophyll triplets in *Heliobacterium chlorum Biochimica et Biophysica Acta 1057*, 346-352.

52.   Kleinherenbrink, F. A. M., Hastings, G., Wittmershaus, B. P., and Blankenship, R. E. (1994) Delayed Fluorescence from Fe-S Type Photosynthetic Reaction Centers at Low Redox Potential, *Biochemistry 33*, 3096-3105.

53.   Trost, J. T., Brune, D. C., and Blankenship, R. E. (1992) Protein sequences and redox titrations indicate that the electron acceptors in reaction centers from heliobacteria are similar to photosystem I, *Photosynth. Res. 32*, 11-22.

54.   Smit, H. W. J., Amesz, J., and Van der Hoeven, M. F. R. (1987) Electron transport and triplet formation in membranes of the photosynthetic bacterium *Heliobacterium chlorum*, *Biochimica et Biophysica Acta 893*, 232-240.

55.   Oh-oka, H., Iwaki, M., and Itoh, S. (2002) Electron donation from membrane-bound cytochrome c to the photosynthetic reaction center in whole cells and isolated membranes of *Heliobacterium gestii*, *Photosynth. Res. 71*, 137-147.

56.   Albert, I., Rutherford, A. W., Grav, H., Kellermann, J., and Michel, H. (1998) The 18 kDa cytochrome c553 from *Heliobacterium gestii*: gene sequence and characterization of the mature protein, *Biochemistry 37*, 9001-9008.

57.   Bominaar, E. L., Ding, X. Q., Gismelseed, A., Bill, E., Winkler, H., Trautwein, A. X., Nasri, H., Fischer, J., and Weiss, R. (1992) Structural, Mossbauer, and EPR investigations on 2 oxidation states of a 5-coordinate, high-spin synthetic heme - Quantitative interpretation of zero-field parameters and large quadrupole splitting, *Inorg. Chem. 31*, 1845-1854.

58.   Degroot, J. J. M., Veldink, G. A., Vliegenthart, J. F. G., Boldingh, J., Wever, R., and Vangelder, B. F. (1975) Demonstration by EPR spectroscopy of functional role of iron in soybean lipoxygenase-1, *Biochimica Et Biophysica Acta 377*, 71-79.

59.   Vassiliev, I. R., Ronan, M. T., Hauska, G., and Golbeck, J. H. (2000) Evidence for an intermediate acceptor F-X in the reaction center of green sulfur bacteria, *Biophys. J. 78*, 784

60.   Hagen, W. R., Eady, R. R., Dunham, W. R., and Haaker, H. (1985) A novel S=3/2 electron paramagnetic res signal associated with the native Fe-proteins of nitrogenase, *FEBS Lett. 189*, 250-254

61.   Leslie Dutton, P. (1978) [23] Redox potentiometry: Determination of midpoint potentials of oxidation-reduction components of biological electron-transfer systems, In *Methods in Enzymology* (Sidney, F., and Lester, P., Eds.), pp 411-435, Academic Press.

62.   Munge, B., Das, S. K., Ilagan, R., Pendon, Z., Yang, J., Frank, H. A., and Rusling, J. F. (2003) Electron transfer reactions of redox cofactors in spinach Photosystem I reaction center protein in lipid films on electrodes, *J. Am. Chem. Soc. 125*, 12457-12463.

63.   Alcantara, K., Munge, B., Pendon, Z., Frank, H. A., and Rusling, J. F. (2006) Thin film voltammetry of spinach photosystem II. Proton-gated electron transfer involving the Mn-4 cluster, *J. Am. Chem. Soc. 128*, 14930-14937.

64. Munge, B., Pendon, Z., Frank, H. A., and Rusling, J. F. (2001) Electrochemical reactions of redox cofactors in *Rhodobacter sphaeroides* reaction center proteins in lipid films, *Bioelectrochemistry 54*, 145-150.

65. Munge, B., Das, S. K., Ilagan, R., Pendon, Z., Yang, J., Frank, H. A., and Rusling, J. F. (2003) Electron transfer reactions of redox cofactors in spinach photosystem I reaction center protein in lipid films on electrodes, *J Am Chem Soc 125*, 12457-12463.

66. Mayhew, S. G. (1978) Redox potential of dithionite and SO2- from equilibrium reactions with flavodoxins, methyl viologen and hydrogen plus hydrogenase, *Eur. J. Biochem. 85*, 535-547.

67. Varadachari, C. G., G; Ghosh, K. (2006) Dissolution of Iron Oxides, *Clay Research 25*, 1-19.

68. Chamorovsky, S. K., and Cammack, R. (1982) Direct determination of the midpoint potential of Acceptor-X in the chloroplast Photosystem I by electrochemical reduction and electron spin resonance spectroscopy, *Photobiochemistry and Photobiophysics 4*, 195-200.

69. Parrett, K. G., Mehari, T., Warren, P. G., and Golbeck, J. H. (1989) Purification and properties of the intact P-700 and Fx-containing Photosystem I core protein, *Biochim Biophys Acta 973*, 324-332.

70. Euro, L., Bloch, D. A., Wikstrom, M., Verkhovsky, M. I., and Verkbovskaya, M. (2008) Electrostatic interactions between FeS clusters in NADH : Ubiquinone oxidoreductase (complex I) from Escherichia coli, *Biochemistry 47*, 3185-3193.

71. Smith, E. T., and Feinberg, B. A. (1990) Redox properties of several bacterial ferredoxins using square-wave voltammetry, *J. Biol. Chem. 265*, 14371-14376.

72. Vassiliev, I. R., Antonkine, M. L., and Golbeck, J. H. (2001) Iron-sulfur clusters in type I reaction centers, *Biochim. Biophys. Acta-Bioenerg. 1507*, 139-160.

73. Sweeney, W. V., and Rabinowitz, J. C. (1980) Proteins containing 4Fe-4S clusters - An overview, *Annu. Rev. Biochem. 49*, 139-161.

74. Karyagina, I., Pushkar, Y., Stehlik, D., van der Est, A., Ishikita, H., Knapp, E. W., Jagannathan, B., Agalarov, R., and Golbeck, J. H. (2007) Contributions of the protein environment to the midpoint potentials of the A1 phylloquinones and the Fx iron-sulfur cluster in photosystem I, *Biochemistry 46*, 10804-10816.

75. Stellwagen, E. (1978) Heme exposure as a determinate of the oxidation-reduction potential of heme proteins, *Nature 275*, 73-74.

76. Kassner, R. J. (1972) Effects of nonpolar environments on redox potentials of heme complexes, *Proc. Natl. Acad. Sci. U. S. A. 69*, 2263

77. Pielak, G. J., Mauk, A. G., and Smith, M. (1985) Site-directed mutagenesis of Cytochrome c shows that an invarieant Phe is not essential for function, *Nature 313*, 152-154.

78.   Evans, M. C. W., Sihra, C. K., Bolton, J. R., and Cammack, R. (1975) Primary electron acceptor complex of photosystem I in spinach chloroplasts, *Nature 256*, 668-670.

79.   Blankenship, R. E. (2010) Early Evolution of Photosynthesis, *Plant Physiol. 154*, 434-438.

80.   Nitschke, W., Setif, P., Liebl, U., Feiler, U., and Rutherford, A. W. (1990) Reaction center photochemistry of *Heliobacterium chlorum*, *Biochemistry 29*, 11079-11088.

81.   Miyamoto, R., Mino, H., Kondo, T., Itoh, S., and Oh-Oka, H. (2008) An electron spin-polarized signal of the P800+A1(Q)- state in the homodimeric reaction center core complex of *Heliobacterium modesticaldum*, *Biochemistry 47*, 4386-4393.

82.   Collins, A. M., Redding, K. E., and Blankenship, R. E. (2010) Modulation of fluorescence in *Heliobacterium modesticaldum* cells, *Photosynth Res 104*, 283-292.

83.   Martin, J. H., Coale, K. H., Johnson, K. S., Fitzwater, S. E., Gordon, R. M., Tanner, S. J., Hunter, C. N., Elrod, V. A., Nowicki, J. L., Coley, T. L., Barber, R. T., Lindley, S., Watson, A. J., Vanscoy, K., Law, C. S., Liddicoat, M. I., Ling, R., Stanton, T., Stockel, J., Collins, C., Anderson, A., Bidigare, R., Ondrusek, M., Latasa, M., Millero, F. J., Lee, K., Yao, W., Zhang, J. Z., Friederich, G., Sakamoto, C., Chavez, F., Buck, K., Kolber, Z., Greene, R., Falkowski, P., Chisholm, S. W., Hoge, F., Swift, R., Yungel, J., Turner, S., Nightingale, P., Hatton, A., Liss, P., and Tindale, N. W. (1994) Testing the iron hypothesis in ecosystems of the equatorial Pacific Ocean, *Nature 371*, 123-129.

84.   Martin, J. H., and Fitzwater, S. E. (1988) Iron-deficiency limits phytoplankton growth in the northeast Pacific Subarctic, *Nature 331*, 341-343.

85.   Chauhan, D., Folea, I. M., Jolley, C. C., Kouril, R., Lubner, C. E., Lin, S., Kolber, D., Wolfe-Simon, F., Golbeck, J. H., Boekema, E. J., and Fromme, P. (2011) A Novel Photosynthetic Strategy for Adaptation to Low-Iron Aquatic Environments, *Biochemistry 50*, 686-692.

86.   Kimble, L. K., Mandelco, L., Woese, C. R., and Madigan, M. T. (1995) *Heliobacterium modesticaldum,* Sp-Nov, A thermophilic heliobactrium of hot springs and volcanic soils, *Archives of Microbiology 163*, 259-267.

87.   Kobayashi, M., Hamano, T., Akiyama, M., Watanabe, T., Inoue, K., Oh-oka, H., Amesz, J., Yamamura, M., and Kise, H. (1998) Light-independent isomerization of bacteriochlorophyll g to chlorophyll a catalyzed by weak acid in vitro, *Analytica Chimica Acta 365*, 199-203.

88.   Heinnickel, M., Shen, G., Agalarov, R., and Golbeck, J. H. (2005) Resolution and reconstitution of a bound Fe-S protein from the photosynthetic reaction center of *Heliobacterium modesticaldum*, *Biochemistry 44*, 9950-9960.

89.   Lefebvre-Legendre, L., Rappaport, F., Finazzi, G., Ceol, M., Grivet, C., Hopfgartner, G., and Rochaix, J. D. (2007) Loss of phylloquinone in Chlamydomonas affects plastoquinone pool size and photosystem II synthesis, *J Biol Chem 282*, 13250-13263.

90.   Wientjes, E., and Croce, R. (2012) PMS: Photosystem I electron donor or fluorescence quencher, *Photosynth. Res. 111*, 185-191.

APPENDIX A

ACS LICENSE

Copyright Clearance Center

RightsLink®

Home | Account Info | Help

ACS Publications
High quality. High impact.

Title: Double Reduction of Plastoquinone to Plastoquinol in Photosystem 1

Author: Michael D. McConnell, John B. Cowgill, Patricia L. Baker, Fabrice Rappaport, and Kevin E. Redding

Publication: Biochemistry

Publisher: American Chemical Society

Date: Dec 1, 2011

Copyright © 2011, American Chemical Society

Logged in as:
john cowgill
Account #:
3000569499

LOGOUT

PERMISSION/LICENSE IS GRANTED FOR YOUR ORDER AT NO CHARGE

This type of permission/license, instead of the standard Terms & Conditions, is sent to you because no fee is being charged for your order. Please note the following:

- Permission is granted for your request in both print and electronic formats, and translations.
- If figures and/or tables were requested, they may be adapted or used in part.
- Please print this page for your records and send a copy of it to your publisher/graduate school.
- Appropriate credit for the requested material should be given as follows: "Reprinted (adapted) with permission from (COMPLETE REFERENCE CITATION). Copyright (YEAR) American Chemical Society." Insert appropriate information in place of the capitalized words.
- One-time permission is granted only for the use specified in your request. No additional uses are granted (such as derivative works or other editions). For any other uses, please submit a new request.

BACK | CLOSE WINDOW

66

APPENDIX B

SPRINGER LICENSE

SPRINGER LICENSE
TERMS AND CONDITIONS

Sep 19, 2012

This is a License Agreement between john cowgill ("You") and Springer ("Springer") provided by Copyright Clearance Center ("CCC"). The license consists of your order details, the terms and conditions provided by Springer, and the payment terms and conditions.

All payments must be made in full to CCC. For payment instructions, please see information listed at the bottom of this form.

License Number	2985550474074
License date	Sep 10, 2012
Licensed content publisher	Springer
Licensed content publication	Photosynthesis Research
Licensed content title	Purification of the photosynthetic reaction center from *Heliobacterium modesticaldum*
Licensed content author	Iosifina Sarrou
Licensed content date	Jan 1, 2012
Volume number	111
Issue number	3
Type of Use	Thesis/Dissertation
Portion	Figures
Author of this Springer article	Yes and you are a contributor of the new work
Order reference number	None
Title of your thesis / dissertation	Characterization of the electron acceptors of the Type-I photosynthetic reaction center of Heliobacterium modesticaldum
Expected completion date	Oct 2012
Estimated size(pages)	60
Total	**0.00 USD**

Terms and Conditions

Introduction
The publisher for this copyrighted material is Springer Science + Business Media. By clicking "accept" in connection with completing this licensing transaction, you agree that the following terms and conditions apply to this transaction (along with the Billing and Payment terms and conditions established by Copyright Clearance Center, Inc. ("CCC"), at the time that you opened your Rightslink account and that are available at any time at http://myaccount.copyright.com).
Limited License
With reference to your request to reprint in your thesis material on which Springer Science and Business Media control the copyright, permission is granted, free of charge, for the use indicated in your enquiry.
Licenses are for one-time use only with a maximum distribution equal to the number that you identified in the licensing process.
This License includes use in an electronic form, provided its password protected or on the university's intranet or repository, including UMI (according to the definition at the Sherpa website: http://www.sherpa.ac.uk/romeo/). For any other electronic use, please contact Springer at (permissions.dordrecht@springer.com or permissions.heidelberg@springer.com).

68